Neutron Stars - dense nuclear matter laboratory

Neutron stars observations and theory of dense nuclear matter

Leszek Zdunik
Centrum Astronomiczne im. M.Kopernika

CAMK
PAN

Seminarium Fizyki Jądra Atomowego, Wydział Fizyki UW, 16.03.2023

Plan

- Neutron star - composition and equation of state
- EOS construction for different density ranges
  - outer crust - nuclei measured in laboratory
  - inner crust - models of nuclei
  - core - extrapolation of nuclear parameters
- Astrophysical measurements
  - masses of neutron stars
    - best-measured binary system with Double Pulsar
    - recent measurement of massive pulsar J0952-0607
  - radius determination (NICER new results)
  - moment of inertia (not measured yet)
  - tidal deformability GW170817 (LIGO/VIRGO measurement)
- Consequences for the theory of dense matter.
  - larger maximum mass ➡ stiffer EOS, phase transition, exotic core.
  - relatively large radius ➡ stiff eos

Neutron stars - observations

$\sim$ 3500 pulsars observed
Electromagnetic - broad range of wavelengths (1967)
Gravitational waves (2017)
Mainly observed in radio:
Pulsars: periods $P = 1.4$ ms - 23 s, $\dot{P} = 10^{-22} - 10^{-10}$

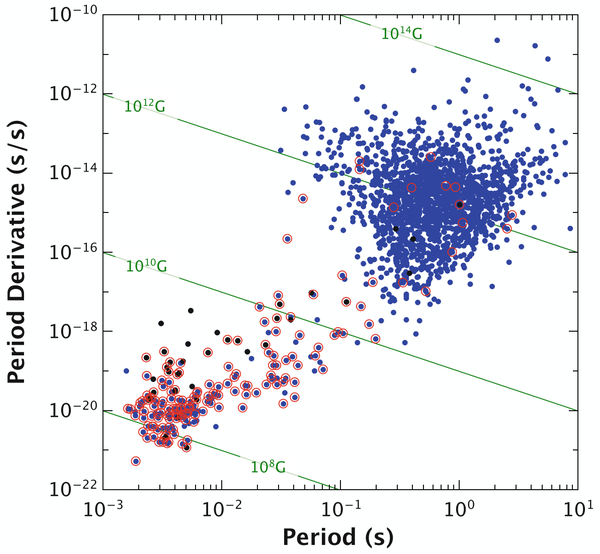

Table 1 Examples of precision measurements for various astrometric and physical quantities, using pulsar timing. A number in brackets indicates the (one-sigma) uncertainty in the last digit(s) of each value

Rotational period of a pulsar:	5.757451924362137(2) ms	PSR J0437−4715	Verbiest et al. (2008)
Distance:	157(1) pc	PSR J0437−4715	Verbiest et al. (2008)
Proper motion in the sky:	140.915(1) mas yr^{-1}	PSR J0437−4715	Verbiest et al. (2008)
Orbital period of a binary pulsar:	1.533449451246(8) d	PSR J1909−3744	Matthews et al. (2015)
Orbital eccentricity:	0.0000749402(6)	PSR J1713+0747	Zhu et al. (2015)
Relativistic periastron advance:	4.226598(5) deg yr^{-1}	PSR B1913+16	Weisberg et al. (2010)
Masses of a neutron stars:	1.4398(2) $M_\odot$	PSR B1913+16	Weisberg et al. (2010)
Mass of a white dwarf:	0.2131(25) $M_\odot$	PSR J1909−3744	Matthews et al. (2015)

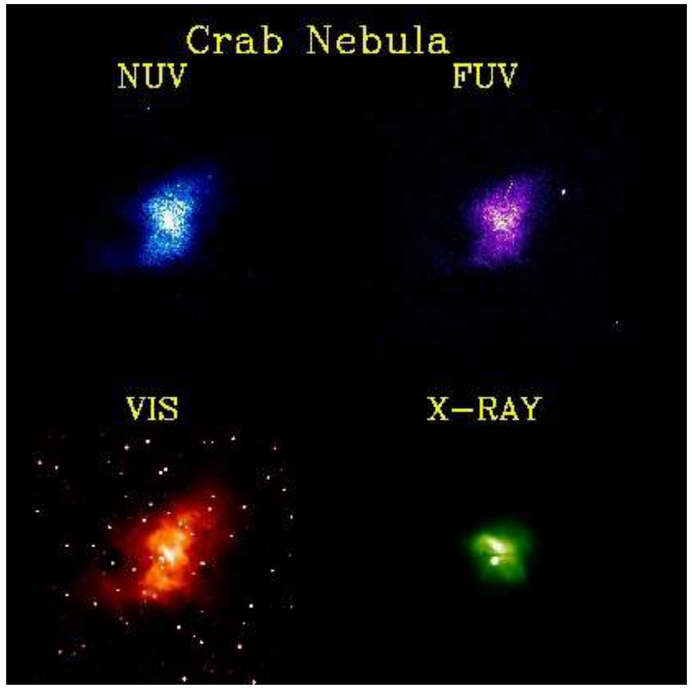

Fig. 1 Period-period derivative diagram for known radio pulsars (Manchester et al. 2005). *Black dots* indicate radio pulsars in globular clusters. *Red circles* indicate radio pulsars in binary systems. The *green lines* give show the estimated surface dipole magnetic field (Lorimer and Kramer 2004)

Neutron star - composition

Outer crust - $\rho < 4 \cdot 10^{11}$ g/cm^3
- nuclei in the electron gas
- neutronization - neutron rich nuclei, Z/A decreases inwards
- neutron drip at the bottom of the outer crust

Inner crust - $4 \cdot 10^{11} < \rho < 10^{14}$ g/cm^3
- nuclei in the electron and neutron gas
- neutronization - neutron rich nuclei

Outer core - $10^{14} < \rho < 5 \cdot 10^{14}$ g/cm^3
- neutrons, protons, electrons, muons

Inner core - $\rho > 5 \cdot 10^{14}$ g/cm^3
- neutrons, protons, electrons, muons
- hyperons ?
- quarks ?

$$M_\odot = 2 \cdot 10^{33}\ \mathrm{g}$$

$\rho_0 \simeq 2.7 \cdot 10^{14}$ g/cm^3 $\quad \rho_0 c^2 = 151$ MeV/fm^3 $\quad n_0 = 0.16$ fm^{-3}

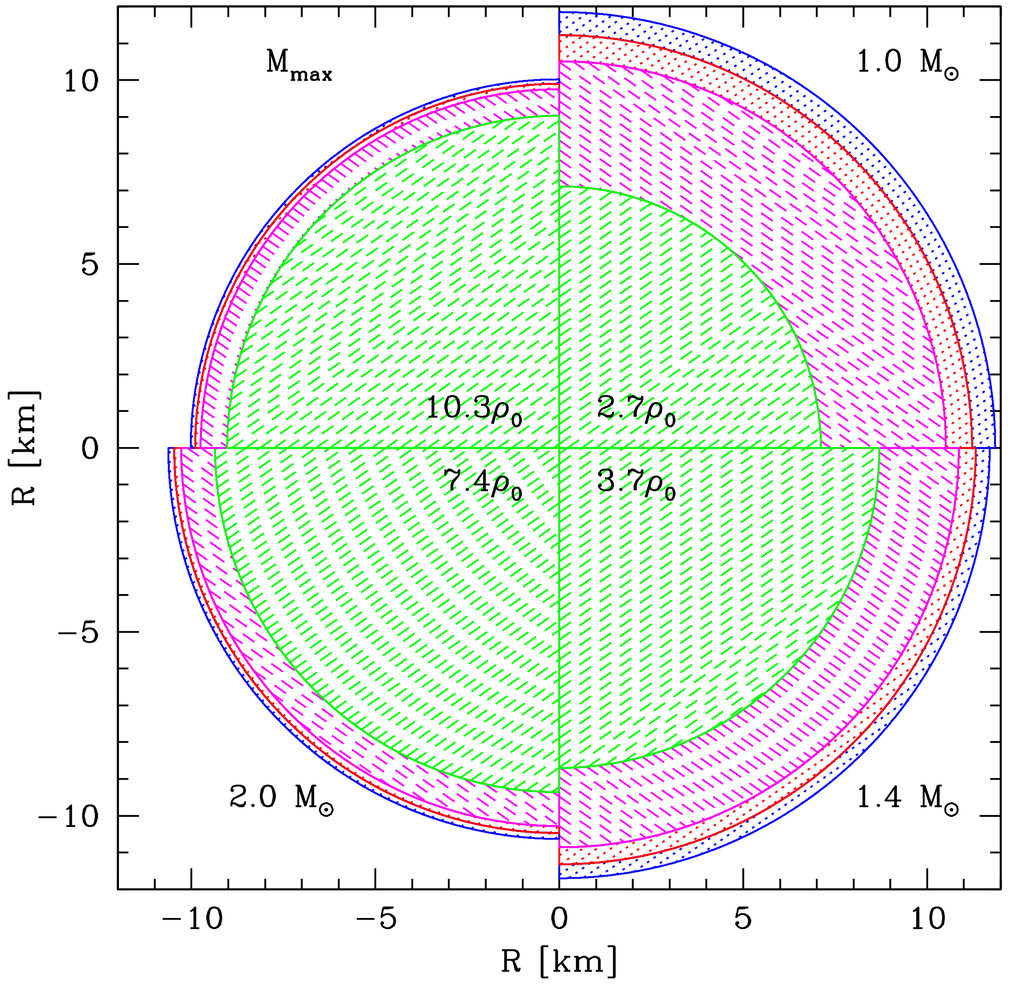

NS crust vs. laboratory measurements

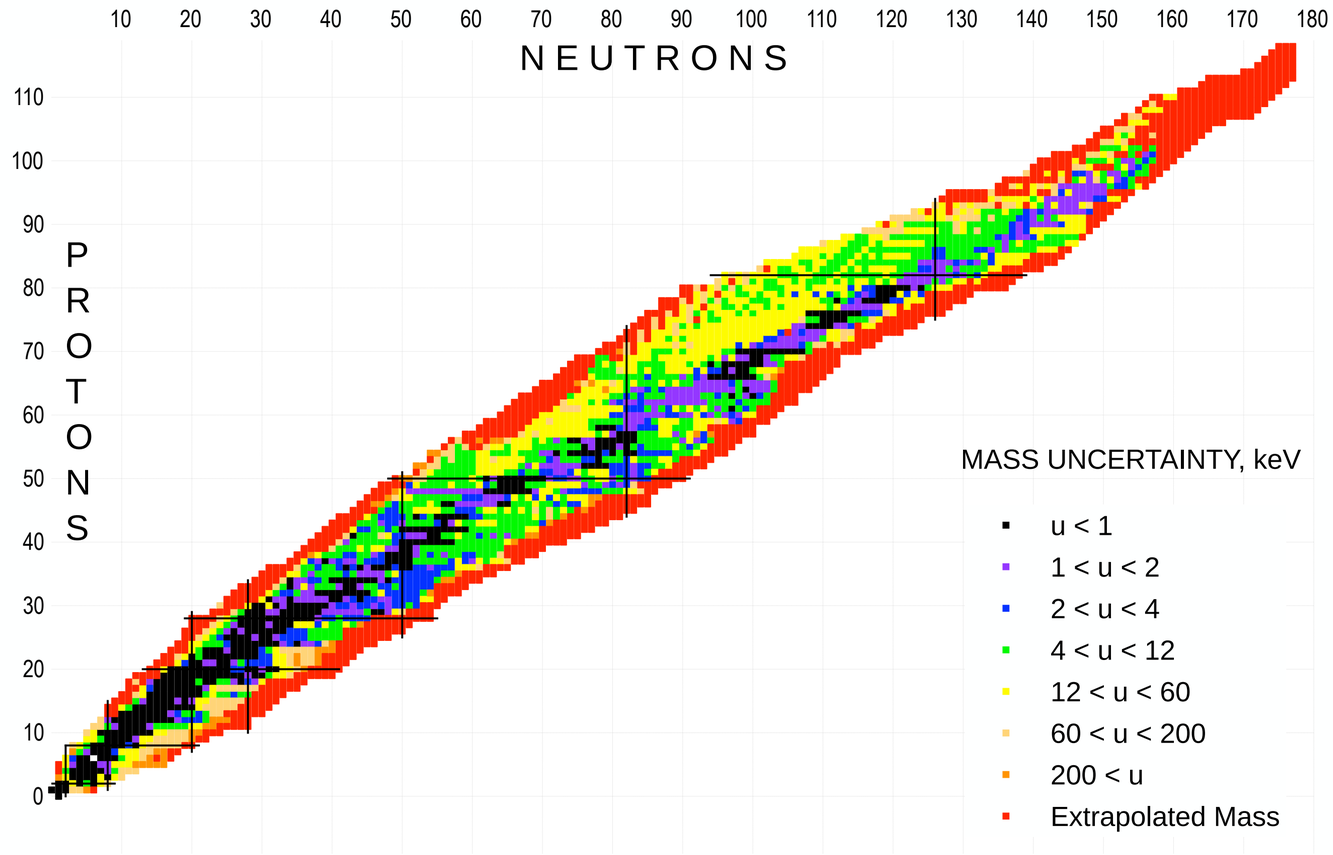

Fig. 1. Nuclear chart displaying the mass-excess uncertainties for all nuclei in their ground state.

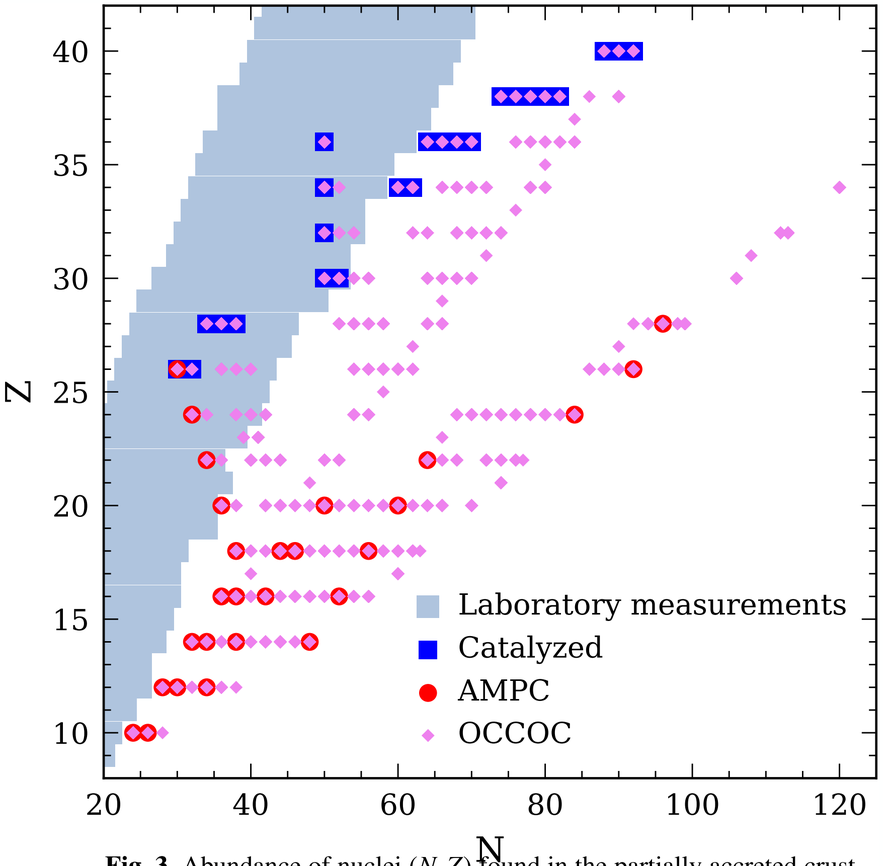

Chinese Physics C Vol. 45, No. 3 (2021) 030001

Fig. 3. Abundance of nuclei (N, Z) found in the partially accreted crust calculated using the Mackie & Baym model, compared to the valley of recently measured nuclei from AME2016. (N, Z) for the catalyzed outer crust are shown in blue, (N, Z) of the accreted material part of the crust are shown in red, and (N, Z) for the originally catalyzed compressed outer crust are shown in violet.

Experimental determination of the binding energy of nuclei

Atomic Mass Evaluation 2020

Suleiman et al.2022

NS mater modelling

- Nuclei - outer crust - up to density $\rho \sim 10^{11}$ g/cm^3 (~ 0.1 MeV/fm^3), pressure $P \sim 10^{29}$ erg/cm^3 ($\sim 10^{-4}$ MeV/fm^3)- experimentally available (measured nuclei). Mass $\Delta M < 10^{-5} M_\odot$, thickness $\Delta R \sim 400$ m.
- Inner part of the outer crust, inner crust, - based on the theory of dense matter and extrapolation of nuclear properties measurements
- Core EOS
  - RMF - relativistic mean-field theory
  - Skyrme density functionals
  - *Ab initio* models

Neutron star - EOS

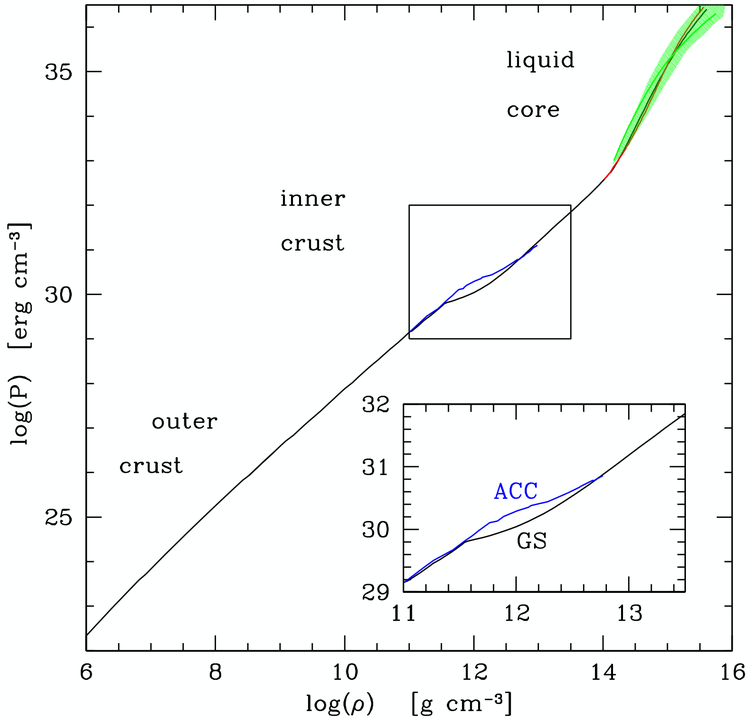

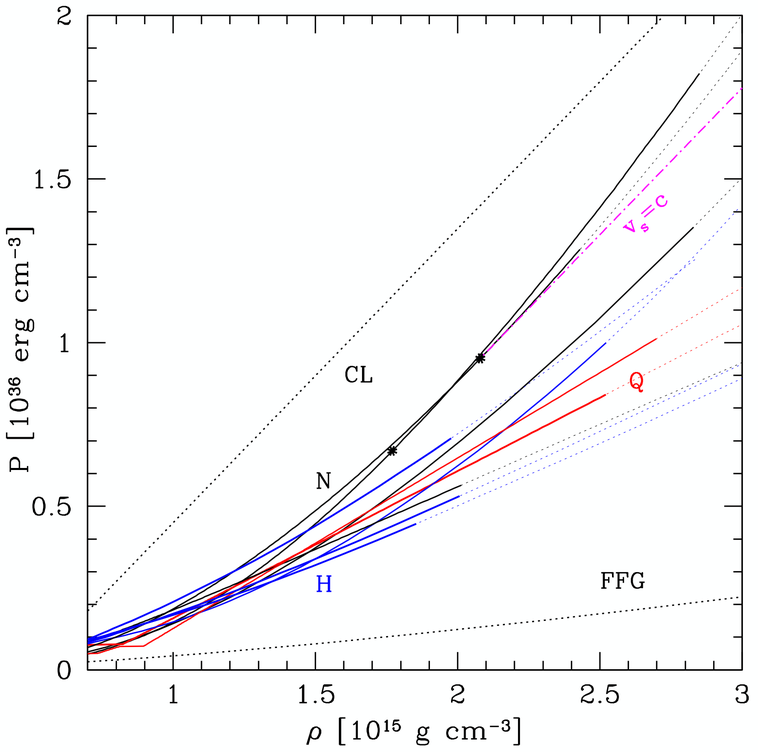

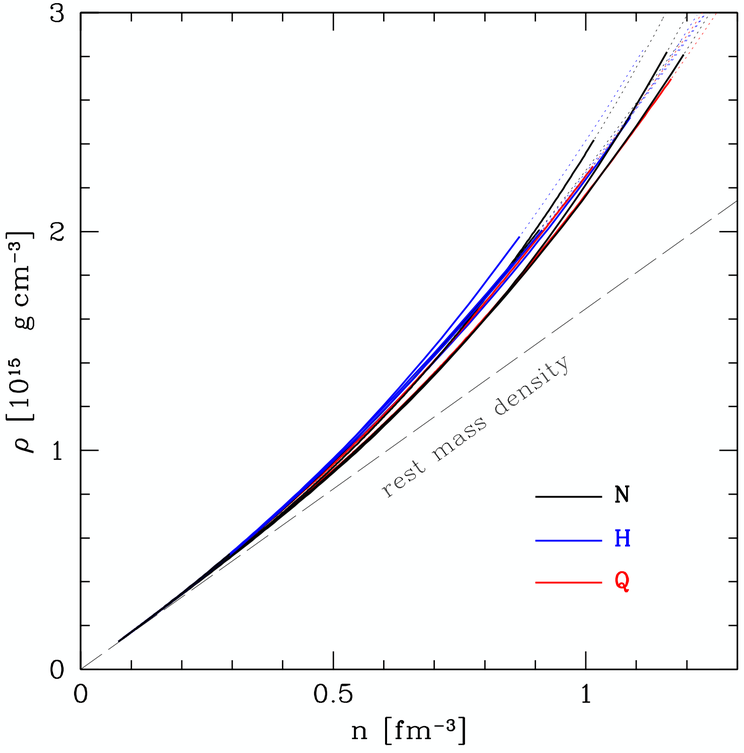

Maximum pressure $\sim 10^{36}$ erg/cm^3 $\simeq$ 624 MeV/fm^3 Maximum density $\sim 2\,10^{15}$ g/cm^3 $\simeq$ 1122 Mev/fm^3

Haensel et al. JoP (2016)

Thermodynamical quantities: pressure P, mass-energy density ρ, baryon number density n

Stiffness and mass-radius relation

Stiffness:

$$v = \sqrt{\frac{dP}{d\rho}} \qquad \Gamma = \frac{\mathrm{d}\log P}{\mathrm{d}\log n}$$

- Stiff EOS - large maximum mass
- repulsion between nucleons necessary to reach large masses
- Fermi gas of neutrons - $M_{\max} \simeq 0.7\, M_{\odot}$

Softening of the EOS:

- weak repulsive forces between nucleons
- phase transitions due to the appearance of hyperons, quarks.

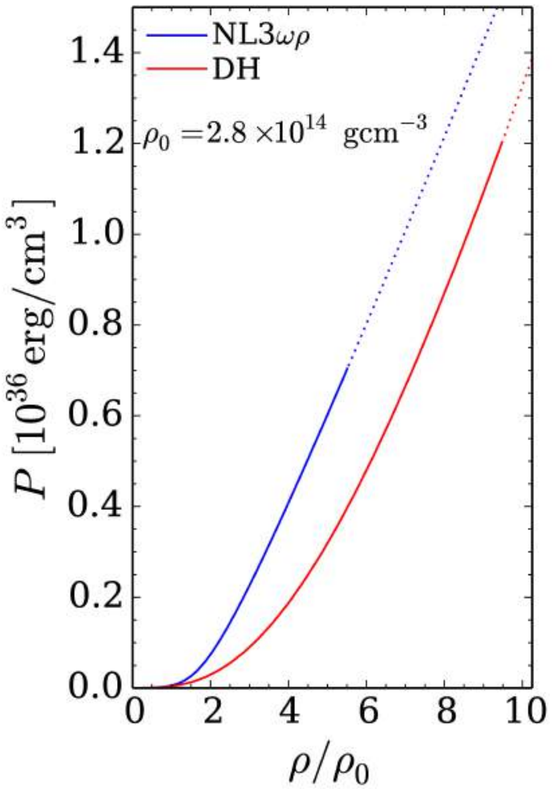

Stiff and soft EOS

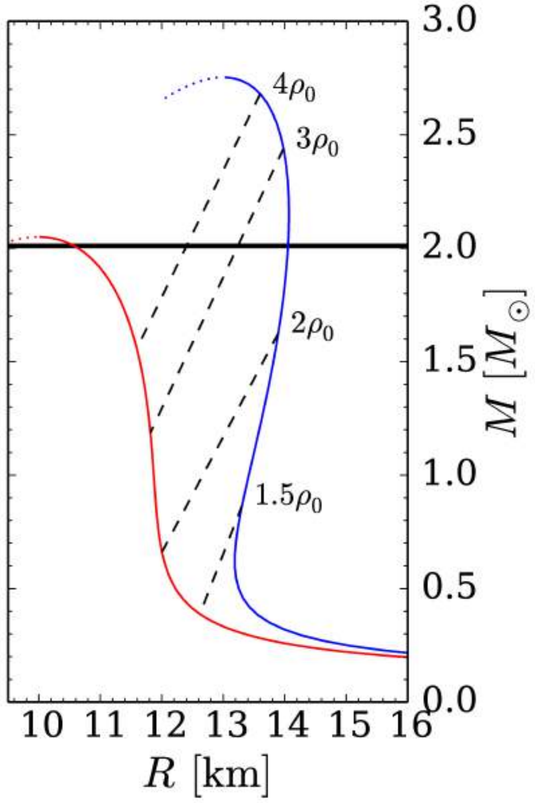

density in the center of NS

Morgane Fortin

Hyperon softening and NS radius

EOS	Theory	Reference
APR	Variational, infinite chain summations	Akmal et al. (1998)
DH	Energy-density functional, Skyrme type	Douchin & Haensel (2001)
BSk20	Energy-density functional, Skyrme type	Fantina et al. (2013)
BM165	RMF, constant couplings, SU(6)	Bednarek et al. (2012)
DS08	RMF, constant couplings, SU(6)	Dexheimer & Schramm (2008)
GM1Z0	RMF, constant couplings, SU(6) broken	Weissenborn et al. (2012)
M.CQMCC	RMF, constant couplings, SU(3)	Miyatsu et al. (2013)
SA.BSR2	RMF, constant couplings, SU(6)	Sulaksono & Agrawal (2012)
SA.TM1	RMF, constant couplings, SU(6) broken	Sulaksono & Agrawal (2012)
G.TM1	RMF, constant couplings, SU(6) broken	Gusakov et al. (2014)
M.TM1C	RMF, constant couplings, SU(3)	Miyatsu et al. (2013)
SA.NL3	RMF, constant couplings, SU(6)	Sulaksono & Agrawal (2012)
M.NL3B	RMF, constant couplings, SU(6)	Miyatsu et al. (2013)
M.GM1C	RMF, constant couplings, SU(3)	Miyatsu et al. (2013)
SA.GM1	RMF, constant couplings, SU(6)	Sulaksono & Agrawal (2012)
UU1	RMF, density-dependent couplings, SU(6)	Uechi & Uechi (2009)
UU2	RMF, density-dependent couplings, SU(6)	Uechi & Uechi (2009)

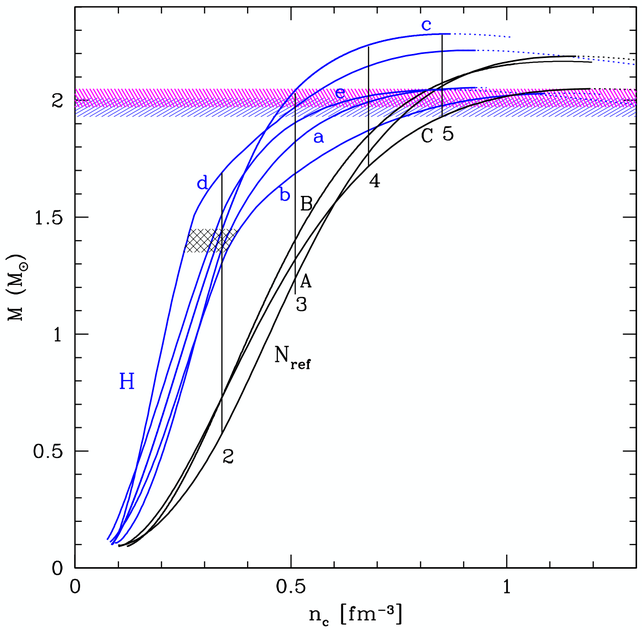

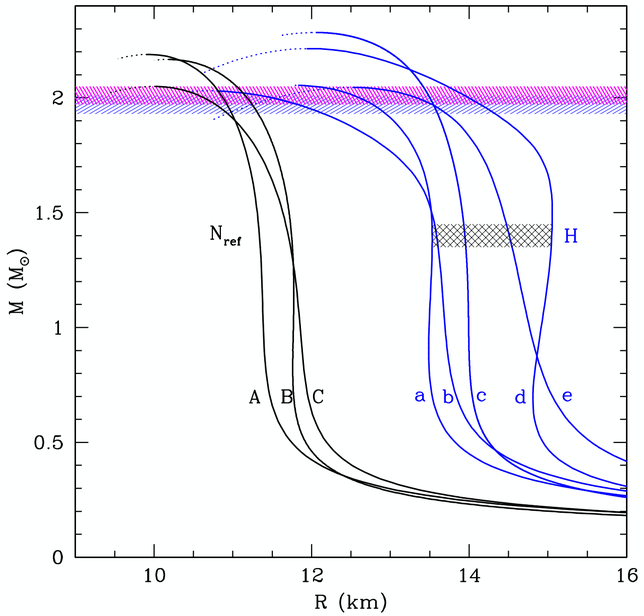

Radii of canonical NS ($M = 1.4\,M_\odot$) are largely determined by the EOS at $\rho_0 - 3\rho_0$

Maximum mass depends on the EOS at $\rho > 3\rho_0$.

To reach high maximum mass softening at high densities ($\rho > 3\rho_0$)

has to be compensated by stiff Eos at $\rho \sim 2\rho_0$.

Astro measurements

Binary Systems Parameters

Keplerian

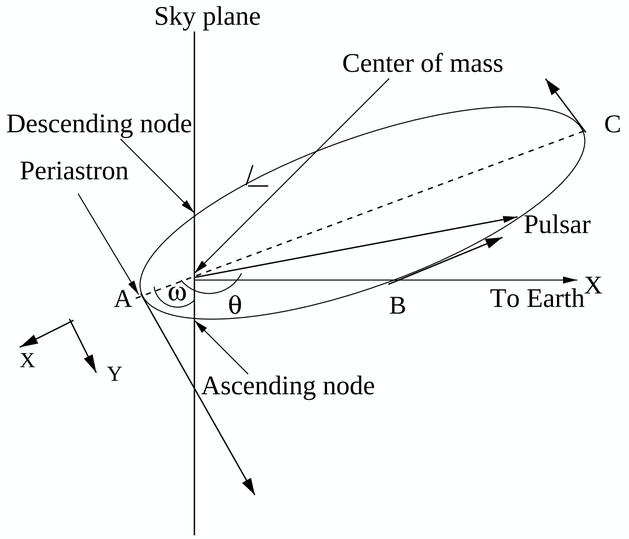

Binary orbit projected to a plane containing the direction of Earth and line of nodes

- Orbital (binary) period P_b
- The orbital eccentricity e
- The projected semi major axis $s = a \sin i$
- The longitude of periastron ω
- The time of periastron passage T_0

Post-Keplerian

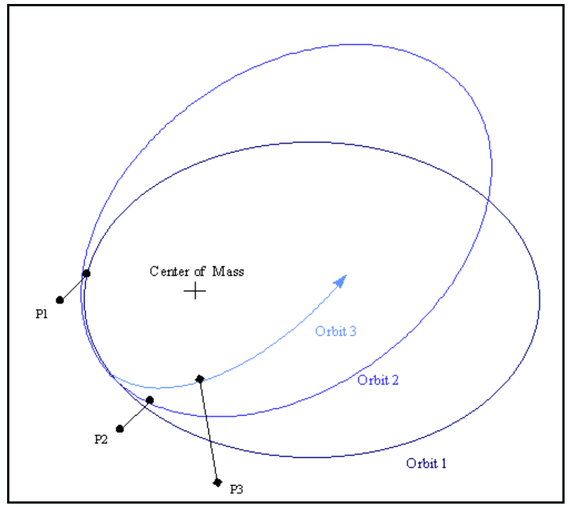

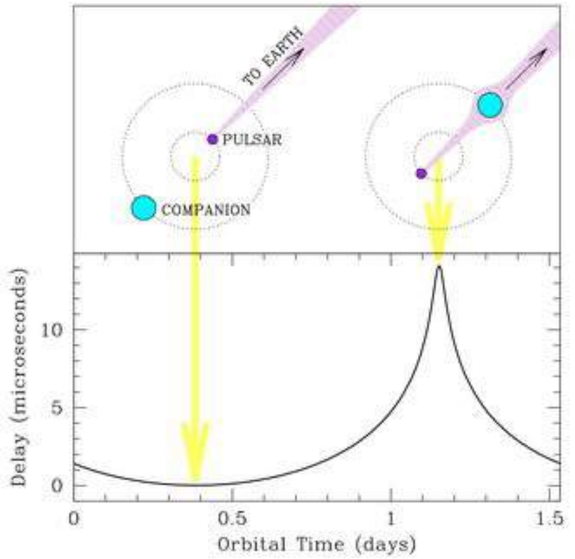

- the rate of orbital decay due to gravitational radiation $\dot{P}_b$
- the relativistic advance of periastron (the relativistic precession of the orbit) $\dot{\omega}$
- the time dilation and gravitational redshift parameter γ
- the Shapiro parameter r (range)
- the Shapiro parameter s (shape)

  r, s a delay that is added to the pulse arrival times when propagating through the curved space-time near the companion

NS mass determination

- Given the precisely measured Keplerian parameters, the only two unknowns are the masses of the pulsar and its companion
- From the measurement of just two PK parameters (eg. $\dot{\omega}$ and γ) one can solve for the 2 masses and then to find the inclination angle
- If more PK parameters measured - system *overdetermined* - can be used to test theory of gravity
- Theory of gravity gives the dependence of PK parameters on masses M_P and M_C
- If two stars (pulsars) observed - additional parameter $R = \dfrac{M_P}{M_c}$

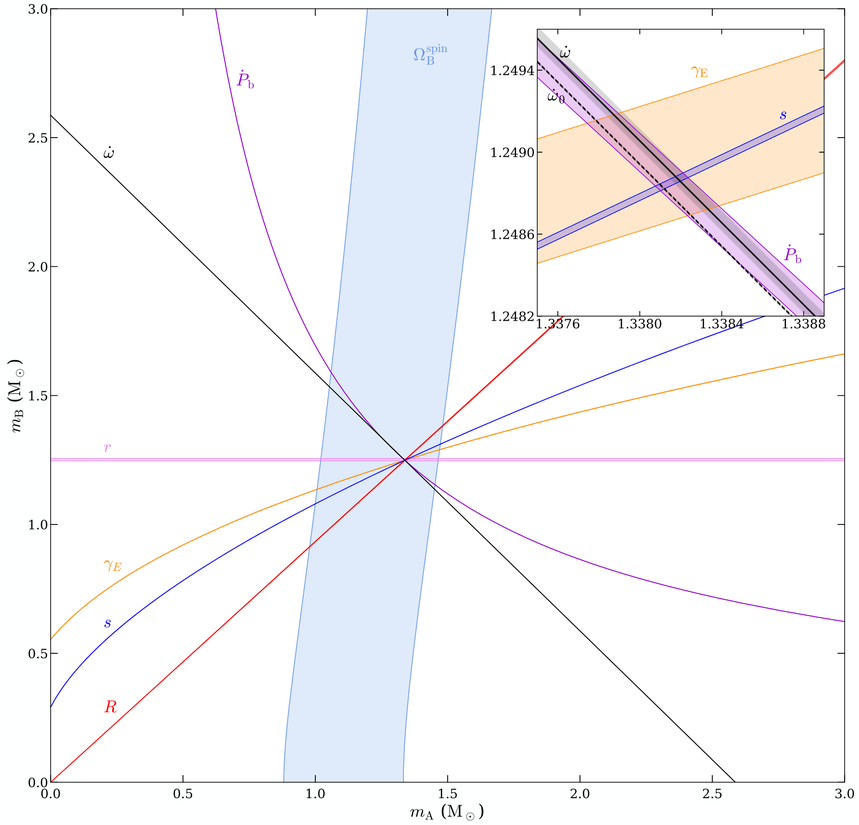

- the rate of orbital decay due to gravitational radiation $\dot{P}_b$
- the relativistic advance of periastron (the relativistic precession of the orbit) $\dot{\omega}$
- the time dilation and gravitational redshift parameter γ
- the Shapiro parameter r (range)
- the Shapiro parameter s (shape)

r, s a delay that is added to the pulse arrival times when propagating through the curved space-time near the companion

Double Pulsar PSR J0737-3039A/B

NS mass measurements

- DNS: double neutron star (NS) systems (the symbol * indicates that the nature of the companion star is unclear: neutron star or massive white dwarf (WD))
- MSP: millisecond pulsars: NSs, not in a DNS, with a rotation period $P \leq 20$ ms (spin frequency $f \geq 50$ Hz) (the symbol † indicates that the companion star is a main-sequence star, unlike for the other systems for which it is a WD)
- SLOW: slowly rotating NSs ($P \geq 20$ ms or $f \leq 50$ Hz), not in a DNS system
- X/OPT.: NSs for which the mass was measured using X-ray or optical observations (while radio timing was used for the other NSs)

errorbars - 1σ

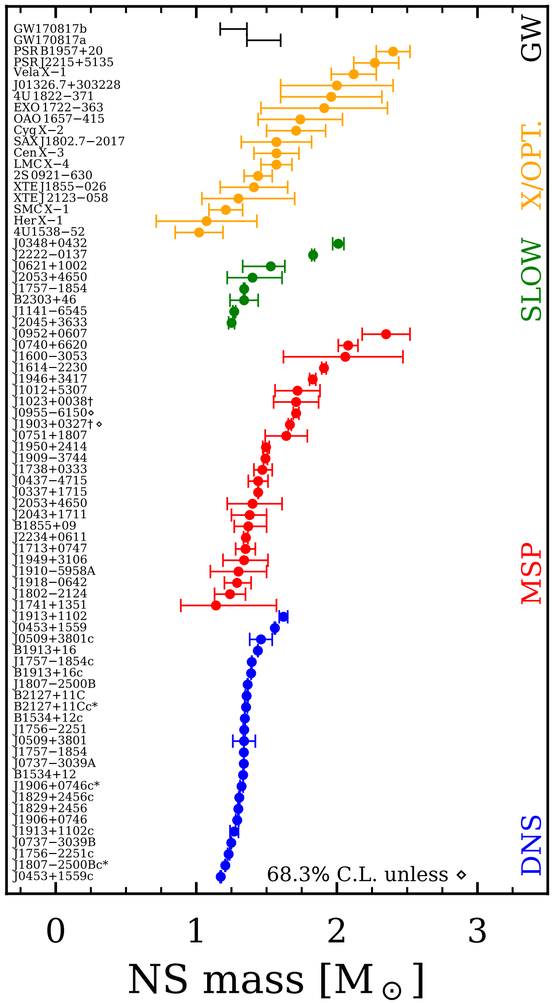

Data available on the website: https://compose.obspm.fr/resources

Suleiman et al. PHYSICAL REVIEW C **104**, 015801 (2021)

NS mass - record holders

system	$M_P(M_\odot)$	$M_P(M_\odot)$ discovery	$M_C(M_\odot)$	$P_b(d)$	$P(ms)$	e	type	discovery
B1913+16	1.43398(2)	1.42	1.39	0.323	59.0	0.617	NS-NS	1974
J0951+1807	1.64(15)	2.1/1.26	0.16	0.263	3.48	$3\ 10^{-6}$	NS-WD	2005/08/16
J1903+0327	1.67(2)	1.74(4)	1.05	95.17	2.15	0.437	NS-MS	2008
J1614-2230	1.908(16)	1.97	0.5	8.7	3.15	$1.3\ 10^{-6}$	NS-WD	2010
J0348+0432	1.97(4)	2.01	0.18	0.102	39.1	$2\ 10^{-6}$	NS-WD	2013
J0740+6620	2.08(7)	2.14	0.26	4.77	2.9	$5\ 10^{-6}$	NS-WD	2019
J0952-0607	2.35(17)	2.35(17)	0.032	0.267	1.41	$<4\ 10^{-3}$	BlackWidow	2017

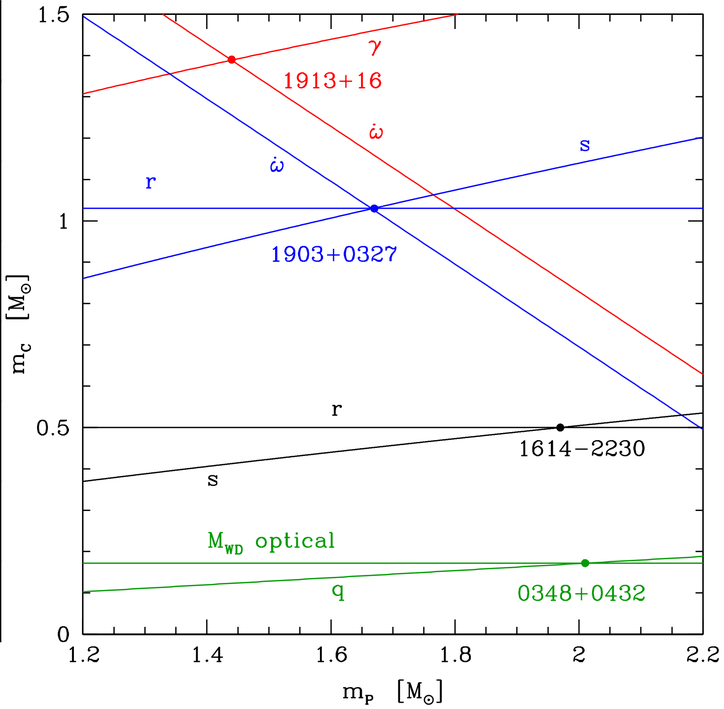

The Astrophysical Journal Letters, 934:L17 (6pp), 2022 August 1 https://doi.org/10.3847/2041-8213/ac8007

PSR J0952−0607: The Fastest and Heaviest Known Galactic Neutron Star

Roger W. Romani[1], D. Kandel[1], Alexei V. Filippenko[2], Thomas G. Brink[2], and WeiKang Zheng[2]
[1] Department of Physics/KIPAC, Stanford University, Stanford, CA 94305, USA; rwr@astro.stanford.edu
[2] Department of Astronomy, University of California, Berkeley, CA 94720-3411, USA
Received 2022 May 12; revised 2022 June 24; accepted 2022 July 4; published 2022 July 26

Abstract

We describe Keck-telescope spectrophotometry and imaging of the companion of the "black widow" pulsar PSR J0952−0607, the fastest known spinning neutron star (NS) in the disk of the Milky Way. The companion is very faint at minimum brightness, presenting observational challenges, but we have measured multicolor light curves and obtained radial velocities over the illuminated "day" half of the orbit. The model fits indicate system inclination $i = 59.^{\circ}8 \pm 1.^{\circ}9$ and a pulsar mass $M_{\rm NS} = 2.35 \pm 0.17\,M_{\odot}$, the largest well-measured mass found to date. Modeling uncertainties are small, since the heating is not extreme; the companion lies well within its Roche lobe and a simple direct-heating model provides the best fit. If the NS started at a typical pulsar birth mass, nearly $1\,M_{\odot}$ has been accreted; this may be connected with the especially low intrinsic dipole surface field, estimated at 6×10^7 G. Joined with reanalysis of other black widow and redback pulsars, we find that the minimum value for the maximum NS mass is $M_{\rm max} > 2.19\,M_{\odot}$ ($2.09\,M_{\odot}$) at 1σ (3σ) confidence. This is $\sim 0.15\,M_{\odot}$ heavier than the lower limit on $M_{\rm max}$ implied by the white dwarf–pulsar binaries measured via radio Shapiro-delay techniques.

Radius measurements

Radius measurements:
- x-ray observations
- Neutron-star Interior Composition Explorer NICER
- Two object measured
- Analysis based on the fitting X-ray emission to the model with two or three emitting spots on the surface of neutron star

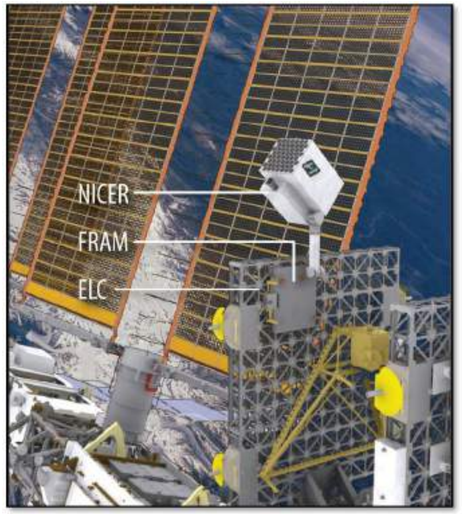

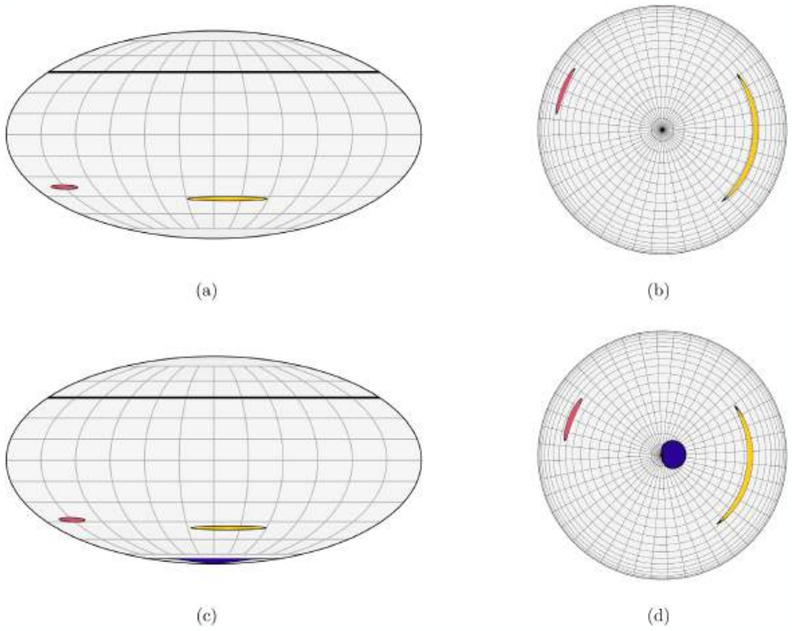

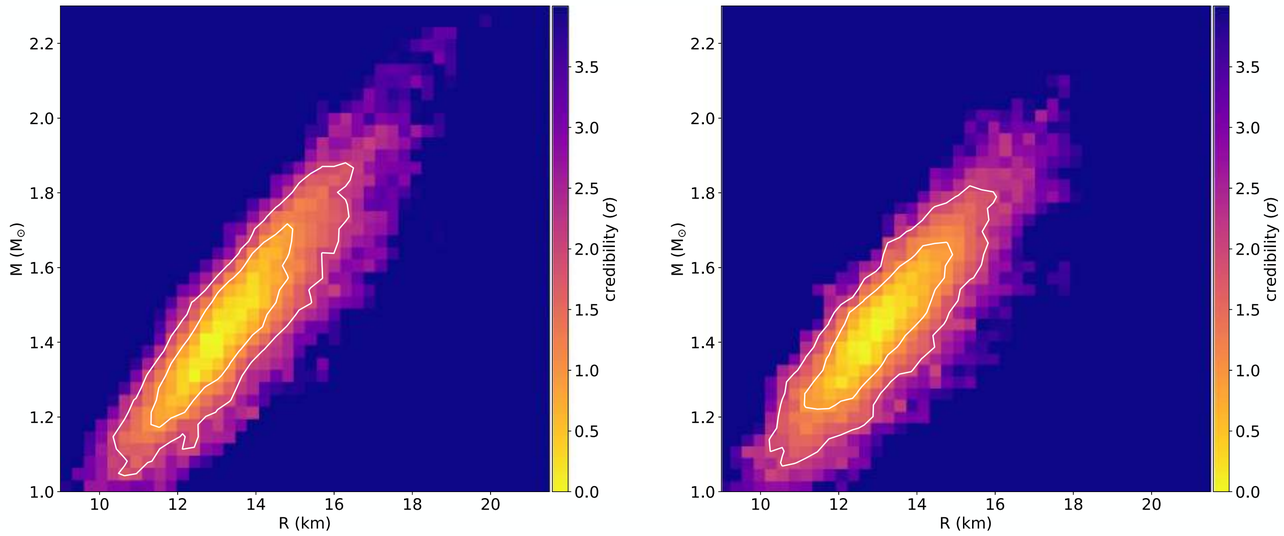

PSR J0030+0451 Mass and Radius from *NICER* Data and Implications for the Properties of Neutron Star Matter

M. C. Miller[1], F. K. Lamb[2,3], A. J. Dittmann[1], S. Bogdanov[4], Z. Arzoumanian[5], K. C. Gendreau[5], S. Guillot[6,7]

Moment of inertia

- Moment of inertia *I* not measured yet

- Some limits on *I* available

- Possibility of *I* measurements for the binary systems
  - relativistic spin-orbit contribution to $\dot{\omega}$

Periastron advance, $\dot{\omega}$ (deg yr^{-1}) [c] 16.899 323(13)

$$\dot{\omega}^{\mathrm{LT,A}} \equiv n_{\mathrm{b}} k^{\mathrm{LT,A}} \simeq -3.77 \times 10^{-4} \times I_{\mathrm{A}}^{(45)} \ \mathrm{deg\ yr}^{-1}$$

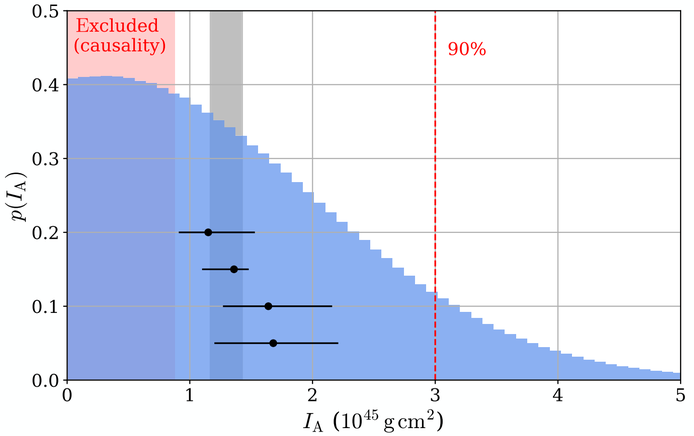

FIG. 8. Probability distribution for the MOI I_{A} of A derived from the $k - s - \dot{P}_{\mathrm{b}}$ test. The vertical dashed red line indicates the upper bound with 90% confidence. $I_{\mathrm{A}} > 0$ is assumed as a prior. The light gray band shows the 90% credible interval one obtains with the limits from Ref. [112] using the radius-MOI relation of Ref. [114]. As a comparison, the horizontal black lines indicate different 90% ranges derived from (top to bottom) tidal-deformability constraints from GW170817 [117], Bayesian modeling of a range of EOSs [116], and two different constraints from NICER observations [118]. The red area is excluded by the causality condition for the EOS [169].

Tidal deformability Λ

Measurable quantities $\mathscr{M}$, $\tilde{\Lambda}$

$$\mathscr{M} = \frac{(M_1 M_2)^{3/5}}{(M_1 + M_2)^{1/5}}$$

$$\tilde{\Lambda} = \frac{16}{13} \frac{\left(M_1 + 12M_2\right) M_1^4 \Lambda_1 + \left(M_2 + 12M_1\right) M_2^4 \Lambda_2}{\left(M_1 + M_2\right)^5}$$

$$\Lambda_i = \frac{2}{3} (GM/Rc^2)^{-5} k_2$$

k_2 - tidal Love number

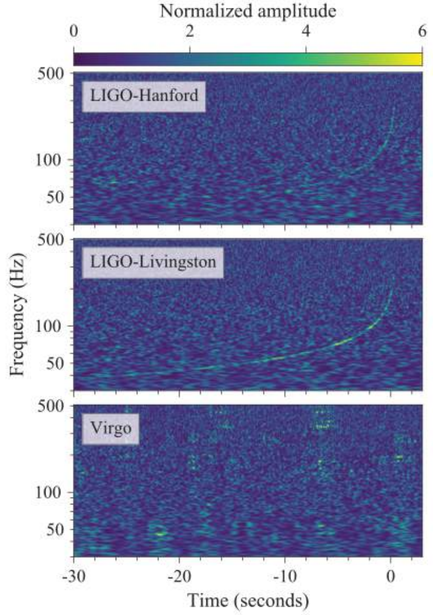

GW170817: $\mathscr{M} = 1.188\, M_\odot \quad \tilde{\Lambda} < 900$

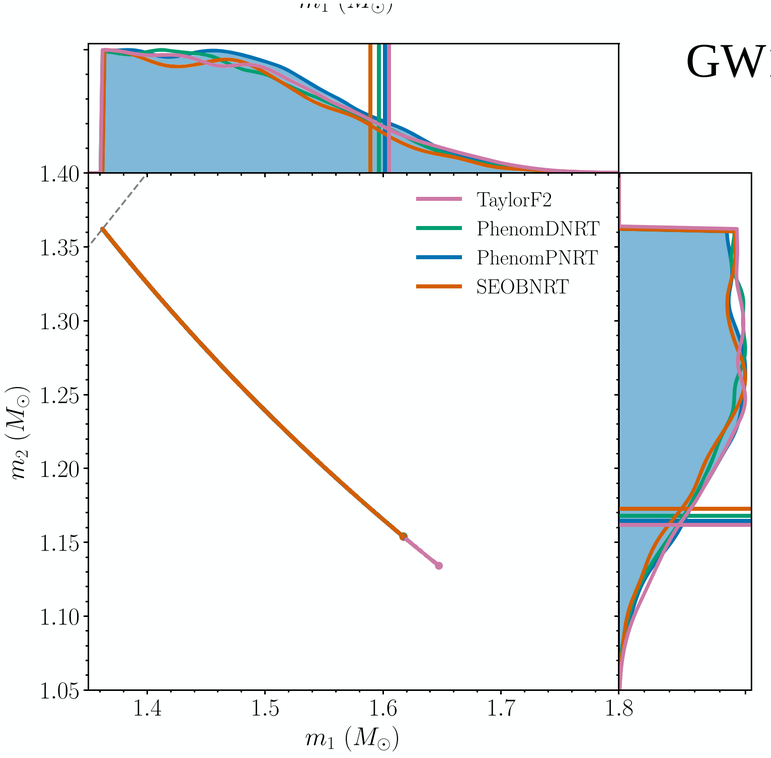

Properties of the Binary Neutron Star Merger GW170817

B. P. Abbott *et al.*[*]
(LIGO Scientific Collaboration and Virgo Collaboration)

FIG. 5. The 90% credible regions for component masses using the four waveform models for the high-spin prior (top panel) and low-spin prior (bottom panel). The true thickness of the contour, determined by the uncertainty in the chirp mass, is too small to show. The points mark the edge of the 90% credible regions. The 1D marginal distributions have been renormalized to have equal maxima, and the vertical and horizontal lines give the 90% upper and lower limits on m_1 and m_2, respectively.

PHYSICAL REVIEW X **9,** 011001 (2019)

FIG. 10. PDFs for the tidal deformability parameters Λ_1 and Λ_2 using the high-spin (top panel) and low-spin (bottom panel) priors. The blue shading is the PDF for the precessing waveform PhenomPNRT. The 50% (dashed lines) and 90% (solid lines) credible regions are shown for the four waveform models. The seven black curves are the tidal parameters for the seven representative EOS models using the masses estimated with the PhenomPNRT model, ending at the $\Lambda_1 = \Lambda_2$ boundary.

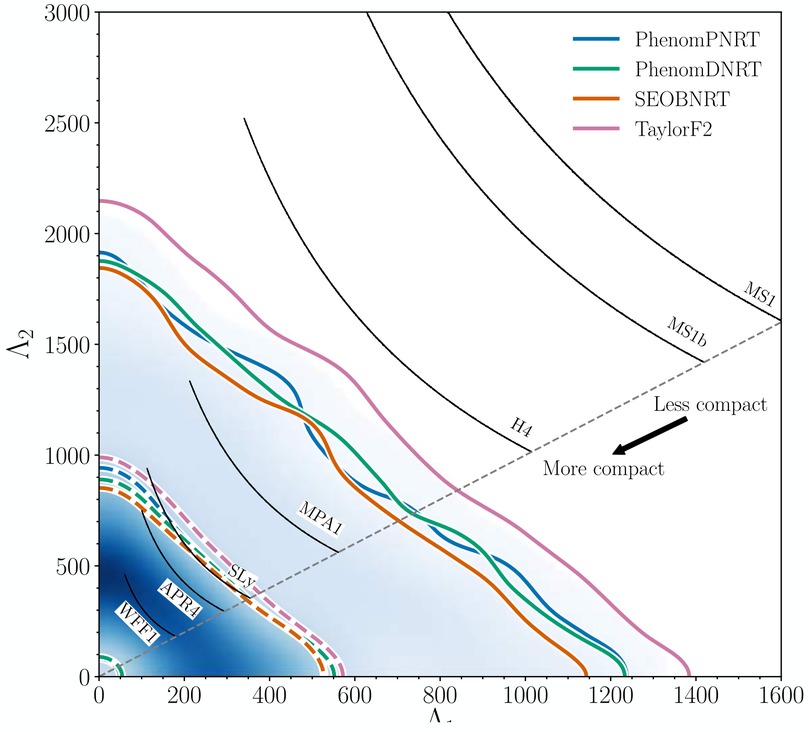

EOS and maximum mass

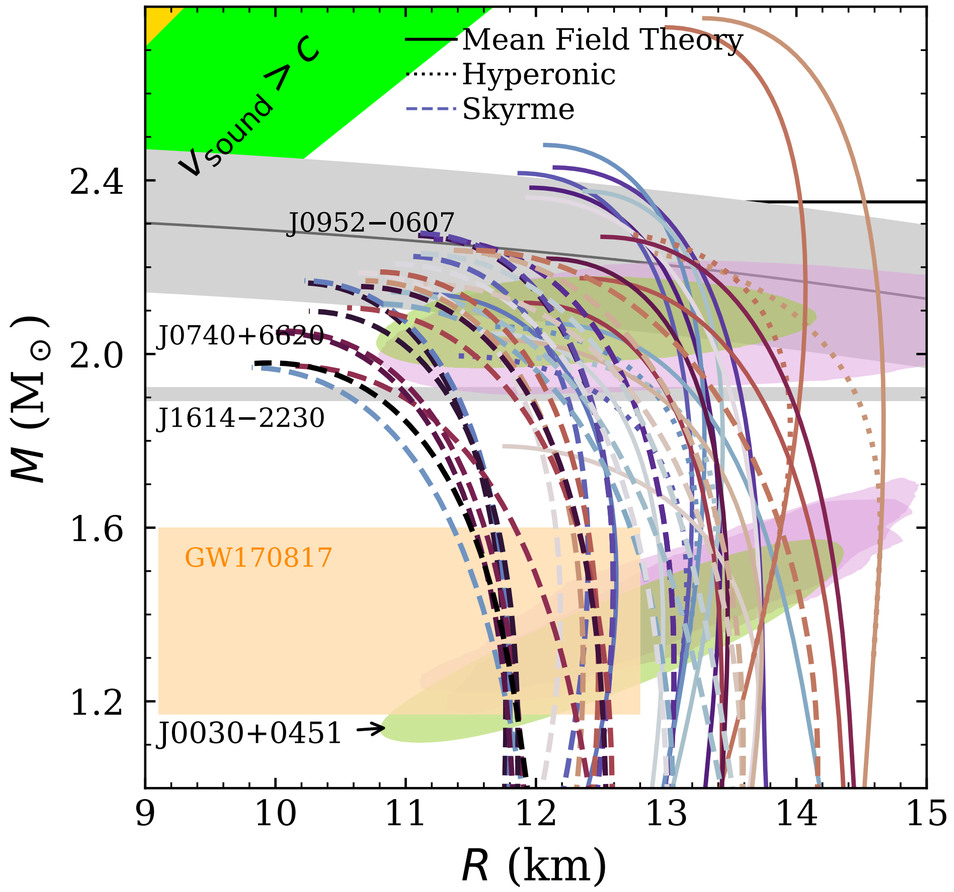

Construction of the Equation of State:
- composition of the core
- nuclear approach in the computations

Composition:
- neutrons, protons, electrons, muons
- hyperons
- deconfined quarks

Nuclear approach:
- Relativistic mean field theory
- Skyrme density functional

Suleiman et al. PHYSICAL REVIEW C **106**, 035805 (2022)

Constraints on symmetry energy parameters

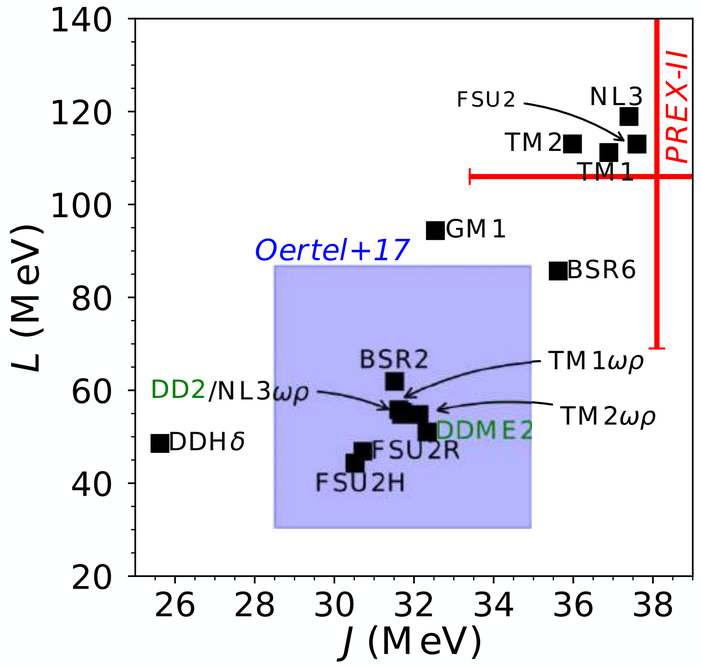

FIG. 5. Symmetry energy and its slope at saturation density respectively denoted J and L for the relativistic mean-field models used in this paper. Experimental data constraints are presented: in blue is the compiled constraint presented in Ref. [42], and in red is that of PREX-II. The names of the EoSs in green refer to nucleonic models that do not permit the direct Urca process.

$$x = n_p/n, \qquad u = n/n_s.$$

$$E(n,x) \simeq E_{1/2}(n) + S(n)(1-2x)^2,$$

$$S_2(n) = (1/8)(\partial^2 E(n,x)/\partial x^2)_{x=1/2}.$$

$$S_v \equiv \frac{1}{8}\left(\frac{\partial^2 E(n,x)}{\partial x^2}\right)_{n_s,1/2} \simeq S(n_s)$$

$$L \equiv \frac{3}{8}\left(\frac{\partial^3 E(n,x)}{\partial n \partial x^2}\right)_{n_s,1/2}.$$

$$S_2(u) \simeq S_v + \frac{L}{3}(u-1) + \frac{K_{sym}}{18}(u-1)^2 + \cdots;$$

J.M. Lattimer, M. Prakash / Physics Reports 621 (2016) 127–164

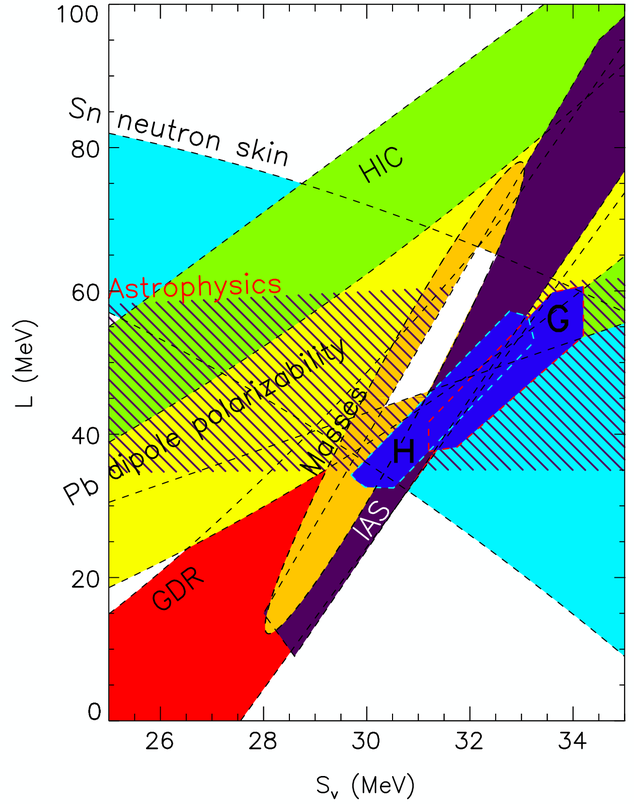

Figure 2. Summary of constraints on symmetry energy parameters. The filled ellipsoid indicates joint S_v–L constraints from nuclear masses (Kortelainen et al. 2010). Filled bands show constraints from neutron skin thicknesses of Sn isotopes (Chen et al. 2010), the dipole polarizability of ^{208}Pb (Piekarewicz et al. 2012), giant dipole resonances (GDR; Trippa et al. 2008), and isotope diffusion in heavy ion collisions (HIC; Tsang et al. 2009). The hatched rectangle shows constraints from fitting astrophysical M–R observations (Steiner et al. 2010, 2013). The two closed regions show neutron matter constraints (H is Hebeler et al. 2010 and G is Gandolfi et al. 2012). The enclosed white area is the experimentally allowed overlap region.

Dense matter at saturation density

Symmetry energy and stellar radius

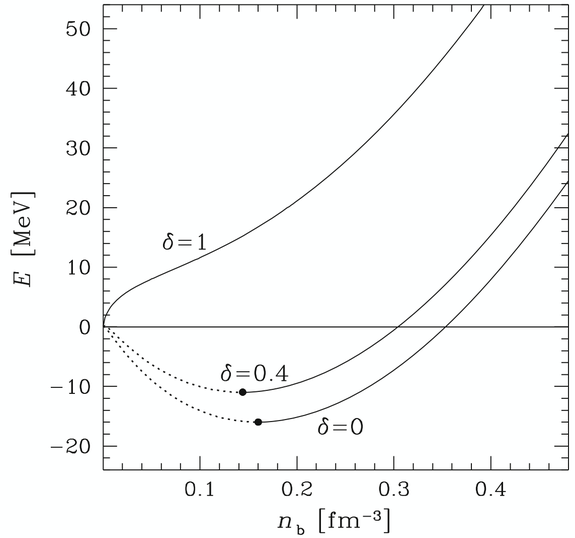

$$n_b = n_n + n_p \qquad \delta = \frac{n_n - n_p}{n_b} \qquad \eta = \frac{n - n_{sat}}{n_{sat}}$$

$$E(n_b, \delta) \simeq E_{sat} + J\delta^2 + \frac{1}{3}L\delta^2\eta + \frac{1}{9}K\eta^2$$

J -symmetry energy, L- slope, K- incompressibility

phenomenological correlations between the pressure of neutron star matter at selected densities, $p_\beta(n)$ in units of MeV fm^{-3}, and the radius of a typical 1.4 $M_\odot$ star[1]

$$R_{1.4} = (9.52 \pm 0.49)[p_\beta(n_s)]^{1/4}\ \text{km};\ R_{1.4} = (5.68 \pm 0.14)[p_\beta(2n_s)]^{1/4}\ \text{km}.$$

$$R_{1.4} \simeq (12.1 \pm 1.1)\ \text{km}$$

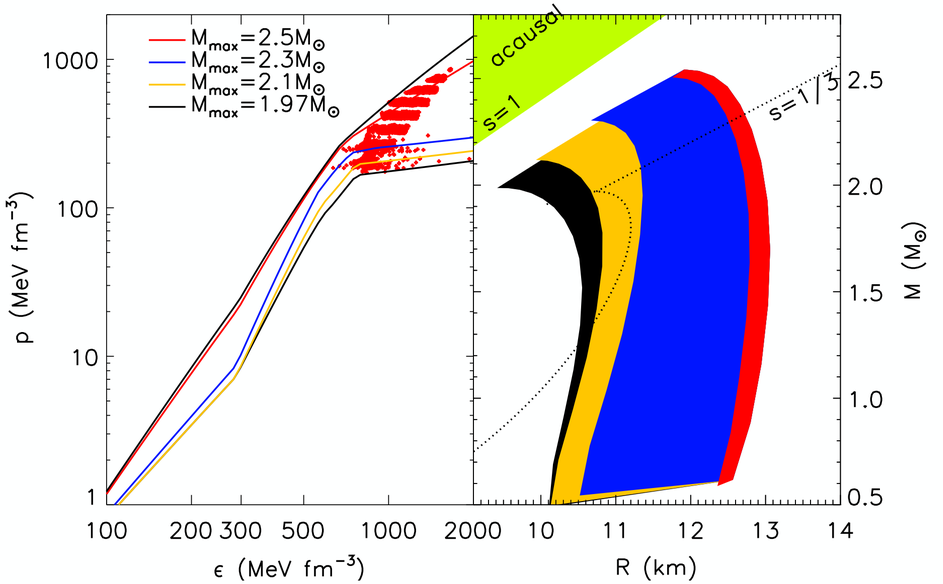

J.M. Lattimer, M. Prakash / Physics Reports 621 (2016) 127–164

MNRAS **519,** 2615–2622 (2023)

Impact of large-mass constraints on the properties of neutron stars

Christian Ecker[1]★ and Luciano Rezzolla[1,2,3]
[1]*Institut für Theoretische Physik, Goethe Universität, Max-von-Laue-Str. 1, 60438 Frankfurt am Main, Germany*
[2]*School of Mathematics, Trinity College, Dublin 2, Ireland*
[3]*Frankfurt Institute for Advanced Studies, Ruth-Moufang-Str. 1, 60438 Frankfurt am Main, Germany*

ABSTRACT

The maximum mass of a non-rotating neutron star, $M_{\rm TOV}$, plays a very important role in deciphering the structure and composition of neutron stars and in revealing the equation of state (EOS) of nuclear matter. Although with a large-error bar, the recent mass estimate for the black-widow binary pulsar PSR J0952–0607, i.e. $M = 2.35 \pm 0.17\,{\rm M}_\odot$, provides the strongest lower bound on $M_{\rm TOV}$ and suggests that neutron stars with very large masses can, in principle, be observed. Adopting an agnostic modelling of the EOS, we study the impact that large masses have on the neutron-star properties. In particular, we show that assuming $M_{\rm TOV} \gtrsim 2.35\,{\rm M}_\odot$ constrains tightly the behaviour of the pressure as a function of the energy density and moves the lower bounds for the stellar radii to values that are significantly larger than those constrained by the NICER measurements, rendering the latter ineffective in constraining the EOS. We also provide updated analytic expressions for the lower bound on the binary tidal deformability in terms of the chirp mass and show how larger bounds on $M_{\rm TOV}$ lead to tighter constraints for this quantity. In addition, we point out a novel quasi-universal relation for the pressure profile inside neutron stars that is only weakly dependent on the EOS and the maximum-mass constraint. Finally, we study how the sound speed and the conformal anomaly are distributed inside neutron stars and show how these quantities depend on the imposed maximum-mass constraints.

Impact of large-mass constraints on the properties of neutron stars

Christian Ecker [1]★ and Luciano Rezzolla

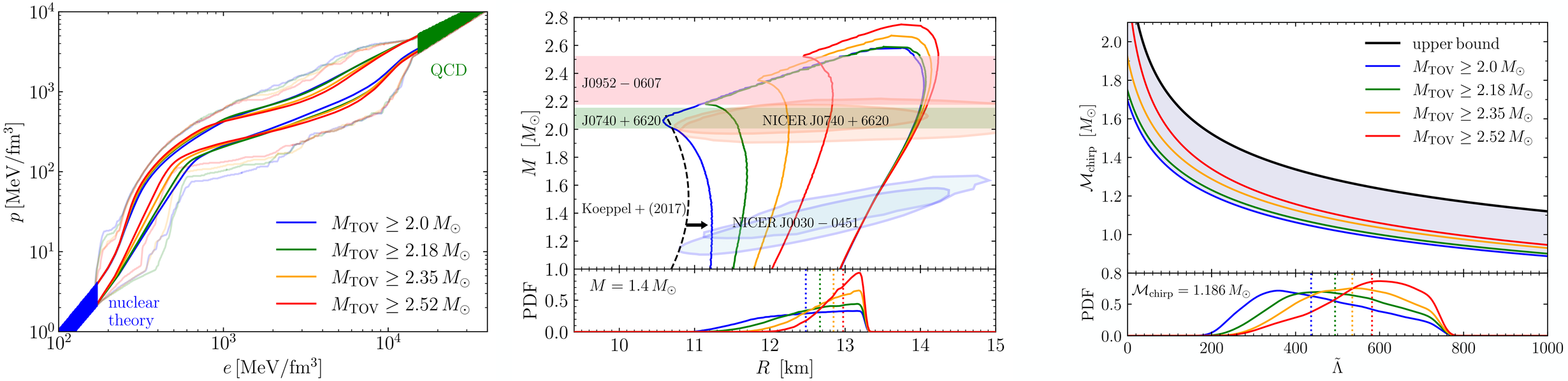

Figure 1. *Left Panel:* PDFs of the various EOSs constructed, with coloured lines showing the 95%-confidence intervals for the different mass constraints Lines with light colours indicate instead the outer boundaries to excluded regions. The blue and green-shaded areas mark the uncertainty of nuclear theory and perturbative QCD, respectively. *Right Panel:* The same as in the left panel but for the PDFs of the mass-radius relations. Blue and orange ellipses are radius measurements of J0030+0451 (Riley et al. 2019; Miller et al. 2019) and of J0740+6620 (Miller et al. 2021; Riley et al. 2021) by the NICER experiment respectively. Green and pink areas are mass measurements of J0740+6620 (Fonseca et al. 2021) and J0952-0607 (Romani et al. 2022), respectively. In the botton part of the panel is reported slices of the PDF for $M = 1.4\,M_\odot$, with the medians being marked by vertical dotted lines.

Figure 2. Relation between the chirp mass and binary tidal deformability. Coloured lines mark lower bounds of the 95 per cent confidence intervals for $\tilde{\Lambda}_{\rm min}$, while the black line is the upper bound $\tilde{\Lambda}_{\rm max}$, which is valid for all mass constraints. In the bottom part of the panel are reported the PDF slices for the measured chirp mass of GW170817 $\mathcal{M}_{\rm chirp} = 1.186\,{\rm M}_\odot$, while the medians are again marked with vertical dotted lines.

the largest bound on the maximum mass coming from PSR J0952-0607 decreases the EOS uncertainty at neutron-star densities significantly, squeezing the 95%-confidence interval for the pressure's PDF to a narrow band around $p \approx 200$ MeV/fm^3 at energy densities $e \approx 600$ MeV/fm^3.

raising the maximum mass bound from 2.0 $M\odot$ to 2.52 $M\odot$ increases systematically the radius of a typical neutron star with 1.4 $M\odot$, taking it from a median value $R_{1.4} = 12.48^{+0.75}_{-1.14}$ km over to $R_{1.4} = 12.97^{+0.28}_{-0.64}$ km, reducing at the same time the 95%-confidence level by almost 50%.

Bayesian approach - example

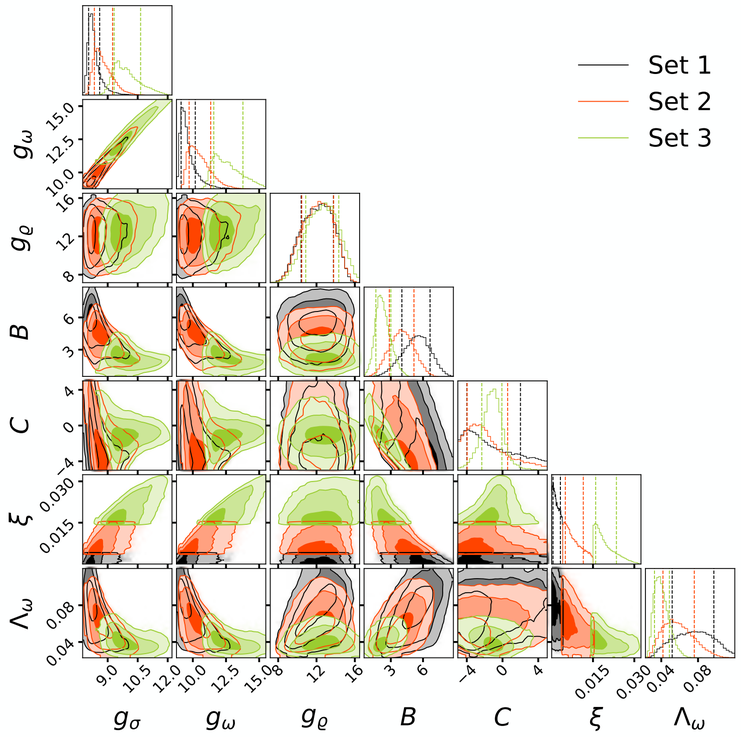

FIG. 2. Corner plot for the three sets of models, set 1 with $\xi \in [0, 0.004]$ (solid black lines), set 2 with $0\xi \in [0.004, 0.015]$ (red) and set 3 with $\xi \in [0.015, 0.04]$ (green), comparing the posteriors of the parameters g_σ, g_ω, g_ρ, $B = b \times 10^3$, $C = c \times 10^3$, and Λ_ω of the RMF model used in present study. The vertical lines represent the 68% CIs, and the different intensities, from dark to light, represent the 1σ, 2σ, and 3σ CIs, respectively.

TABLE II. The constraints imposed in the Bayesian inference to generate all sets of models: binding energy per nucleon ϵ_0, incompressibility K_0, symmetry energy $J_{\mathrm{sym},0}$ at the nuclear saturation density ρ_0, including an 1σ uncertainty; the pressure of pure neutron matter PNM determined at the densities 0.08, 0.12 and 0.16 fm^{-3} from a χEFT calculation [38], with $2 \times$ N^{3}LO uncertainty in the likelihood, the pressure of PNM is an increasing function of density and the maximum NS mass above $2M_\odot$.

Constraints			
Quantity		Value/Band	Ref
NMP [MeV]	ρ_0	0.153 ± 0.005	[19]
	ϵ_0	-16.1 ± 0.2	[42]
	K_0	230 ± 40	[18, 43]
	$J_{\mathrm{sym},0}$	32.5 ± 1.8	[44]
PNM [MeV fm^{-3}]	$P(\rho)$	$2\times$ N^{3}LO	[38]
	$dP/d\rho$	> 0	
NS mass $[M_\odot]$	M_{max}	> 2.0	[45]

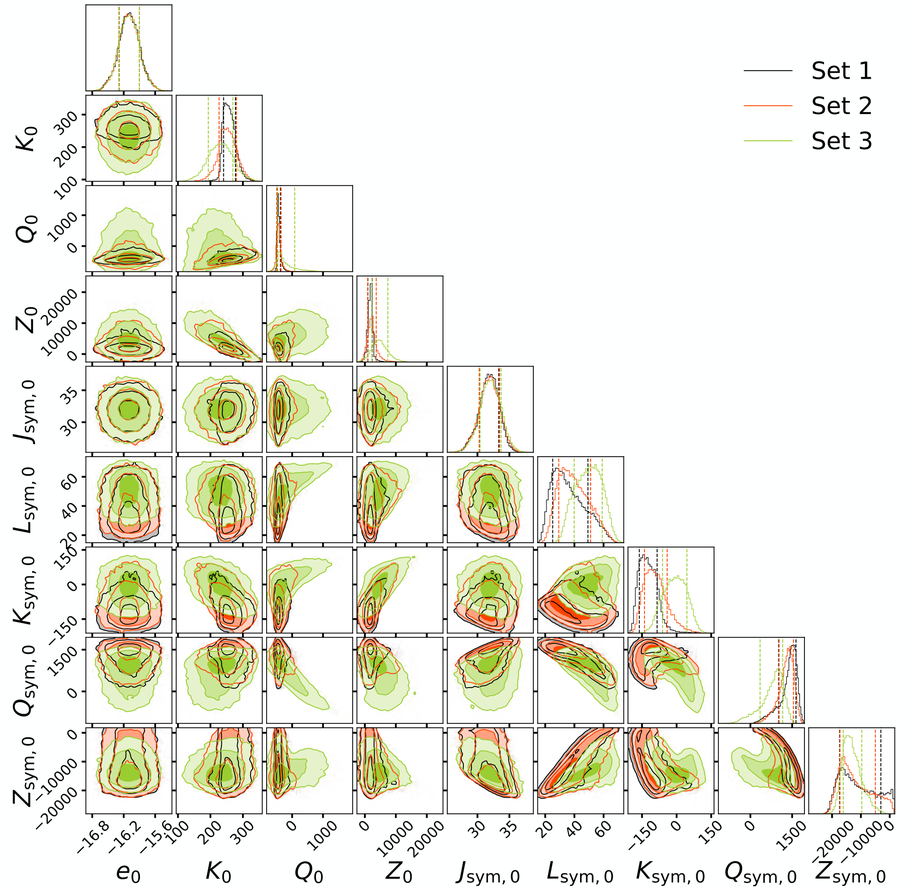

FIG. 4. Corner plot for the three sets of models with $\xi \in [0, 0.004]$ (solid black lines), $\xi \in [0.004, 0.015]$ (red) and $\xi \in [0.015, 0.04]$ (green) comparing the respective nuclear matter properties, in particular, the binding energy ϵ_0, incompressibility K_0, skewness Q_0 and curtosis Z_0 at saturation that characterize symmetric nuclear matter and symmetry energy $J_{\mathrm{sym},0}$, its slope $L_{\mathrm{sym},0}$, curvature $K_{\mathrm{sym},0}$, skewness $Q_{\mathrm{sym},0}$ and curtosis Z_{sym} at saturation that characterizes the symmetry energy. The vertical lines represent the 68% CIs, and the light and dark intensities represent the 1σ, 2σ, and 3σ CIs, respectively.

Spanning the full range of neutron star properties within a microscopic description

- Malik, Tuhin; Ferreira, Márcio; Bastos Albino, Milena; Providência, Constança arXiv:2301.08169 2023

Bayesian approach - example

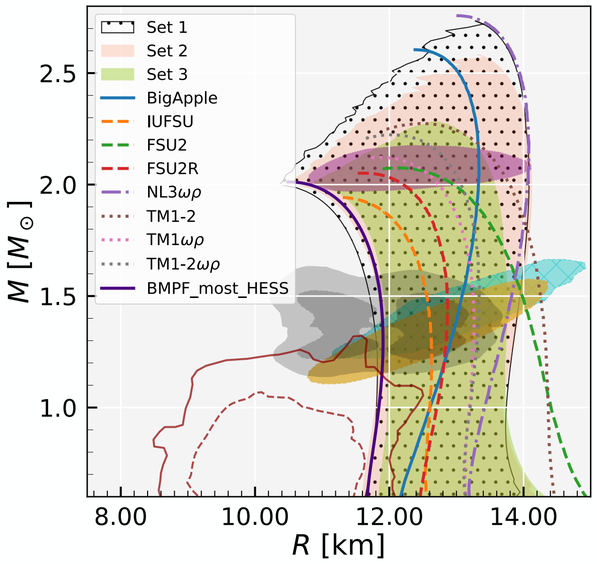

FIG. 6. NS mass-radius domains (full posterior) produced in the following three scenarios: set 1 with $\xi \in [0, 0.004]$ (black dot), set 2 with $\xi \in [0.004, 0.015]$ (salmon), and set 3 with $\xi \in [0.015, 0.04]$ (green). The gray lines depict the constraints from the binary components of GW170817, along with their 90% and 50% credible intervals (CI). The 1σ (68%) CI for the 2D posterior distribution in the mass-radii domain for millisecond pulsar PSR J0030 + 0451 (cyan and yellow) [46, 47] as well as PSR J0740 + 6620 (violet) [48, 49] from the NICER x-ray data are also shown. Additionally, we show the constraint obtained from HESS J1731-347 for 68.3% (95.4%) CIs in dashed dark red (solid dark red) [50]. MR curves from a few well-known RMF models are also plotted (see text for details). Also, shown is BMPF_most_HESS, the EoS from our complete set that best describes HESS J1731-347.

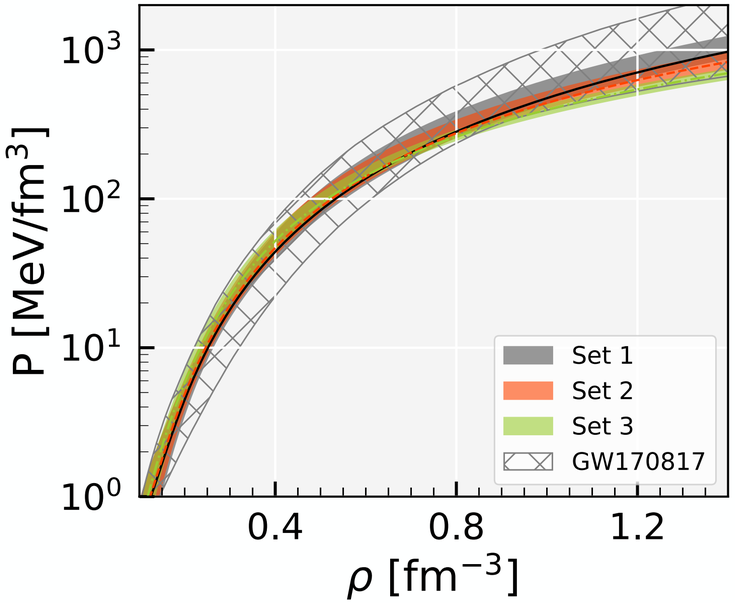

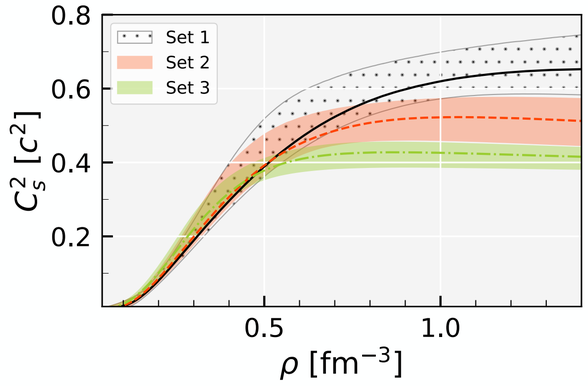

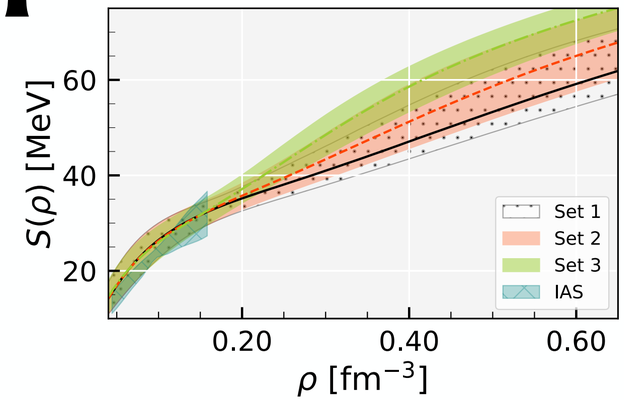

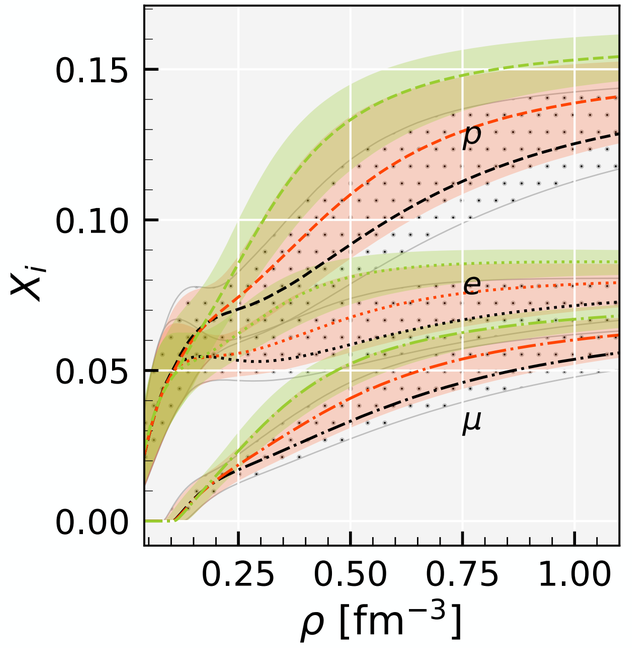

Spanning the full range of neutron star properties within a microscopic description

Tuhin Malik,[1,*] Ma´rcio Ferreira,[1,†] and Constanc¸a Provide^ncia[1,‡] [1]*CFisUC, Department of Physics, University of Coimbra, 3004-516 Coimbra, Portugal.*

EOS with phase transition/softening

And M (R) relation

Softening of the EOS:

- Smaller maximum mass
- Configurations with similar mass and different radius
- *Strong* phase transition - possibility of the existence of *twins* - the same mass and different structure and size

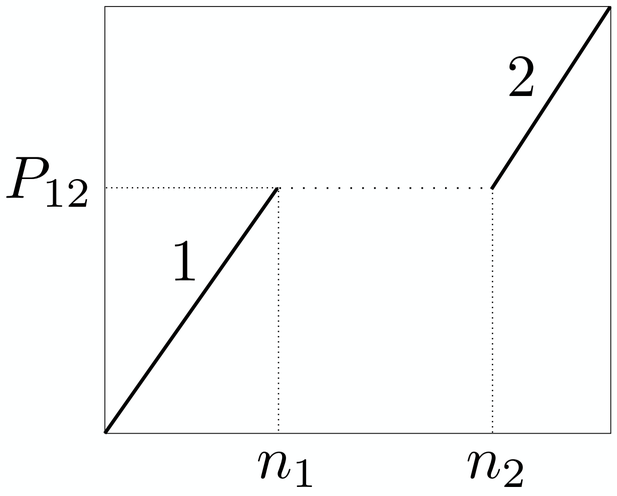

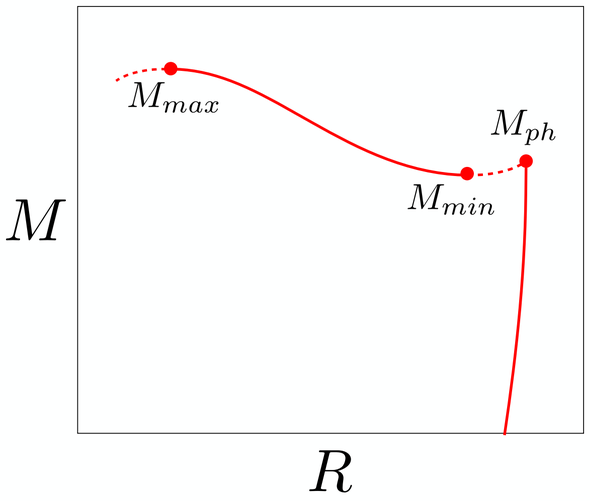

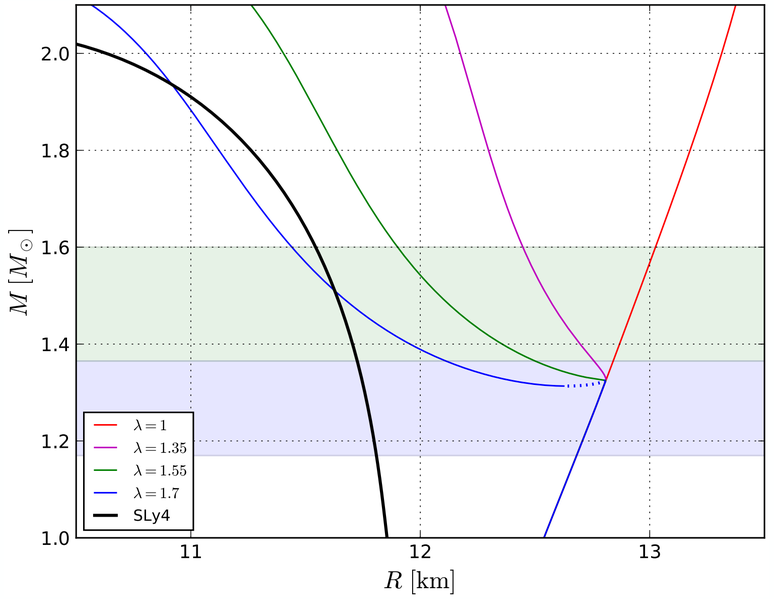

Fig. 7. Mass-radius relations for the polytropic-quark EOS with realistic SLy4 crust. Selected $M(R)$ relations correspond to a polytropic segment of $\gamma = 4.5$, connected to the SLy4 crust at $n_0 = 0.21\,\mathrm{fm}^{-3}$ and to a linear EOS of $\alpha = 1$ (Eq. (2)) at $n_1 = 0.335\,\mathrm{fm}^{-3}$. The curves differ by the density jump $\lambda = n_2/n_1$, as indicated in the plot. Regions destabilised by the phase transition are indicated by dotted segments. The black line indicates the SLy4 EOS. The pale green and blue bands correspond to the mass ranges estimated in the low-spin prior case of GW170817 (Abbott et al. 2017).

EOS with phase transition/softening

And M (R) relation

Phase transition in the center of NS:

- Softening due to the phase transition for the first order phase transition

$$\frac{dM}{d\rho_{c+}} \simeq (3 - 2\lambda + 3P_{pt}/\rho_{pt})\frac{dM}{d\rho_{c-}}$$

- Increase of a stiffness needed to reach large M_{max}

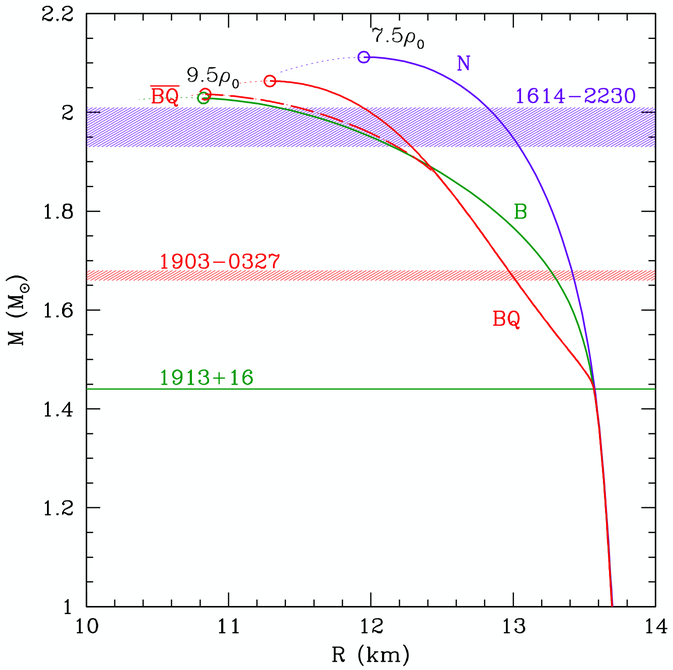

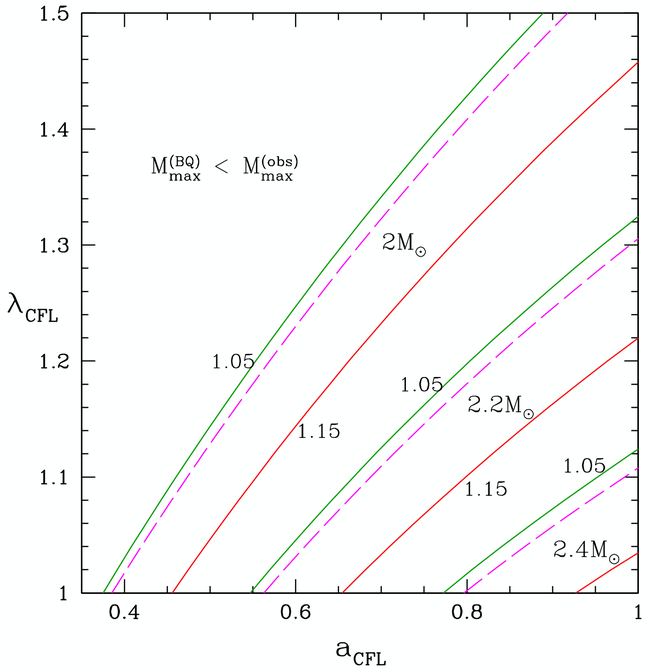

Larger λ → Larger stiffness above phase transition point $a = c_s^2$

Phase transition and observations

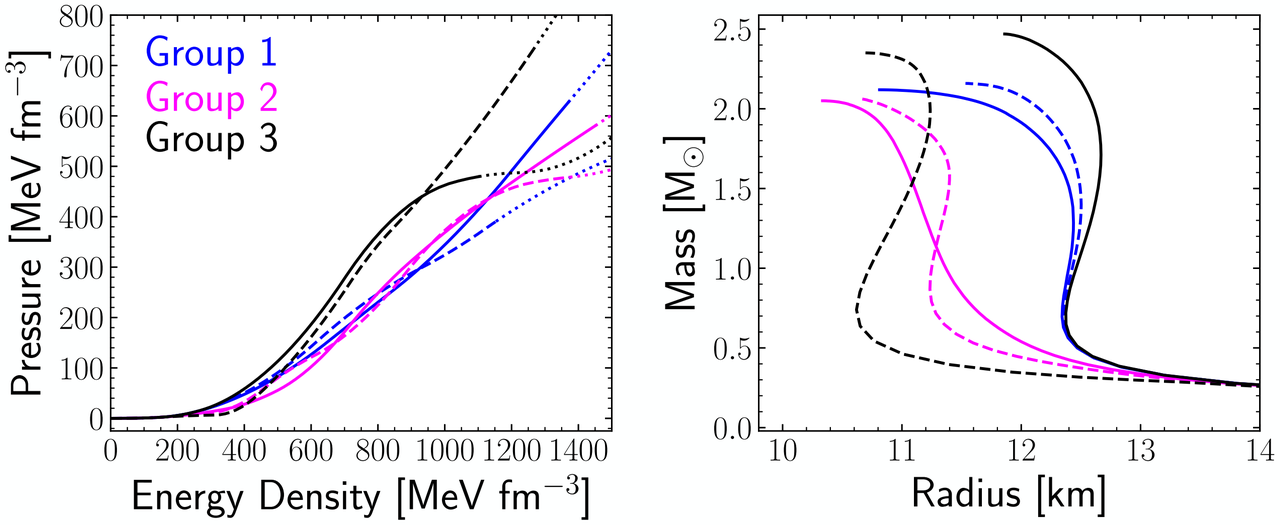

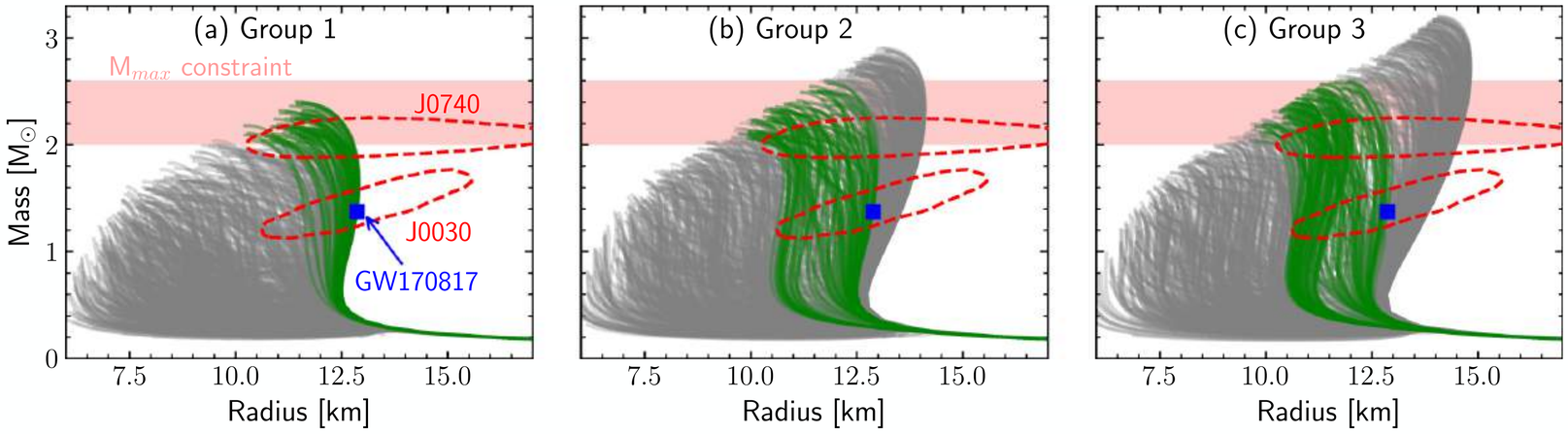

Current observations does not favour exotic matter over the standard hadronic matter

(1) group 1 contains EoSs whose maximal slope is less than three times the slope at $n_{\rm sat}$, $c'_{\rm max} \leqslant 3c'_{\rm sat}$,
(2) group 2 contains all EoSs with $3c'_{\rm sat} < c'_{\rm max} \leqslant 6c'_{\rm sat}$,
(3) and group 3 contains all EoSs with $6c'_{\rm sat} < c'_{\rm max} \leqslant 9c'_{\rm sat}$.

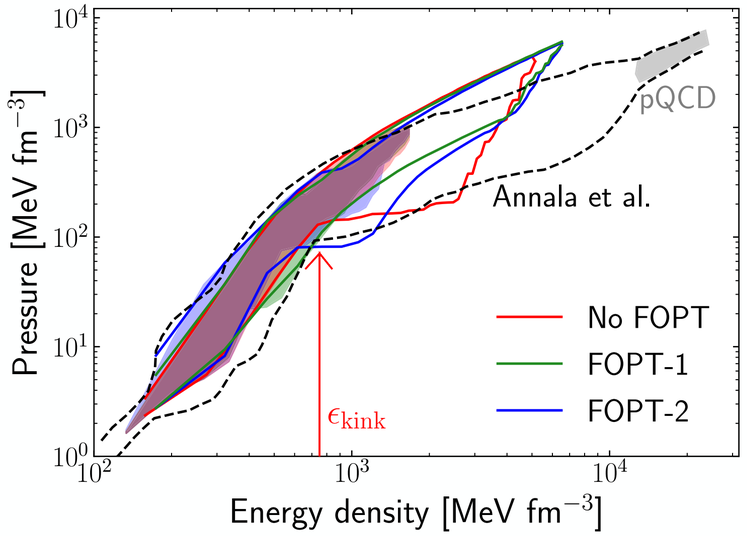

FIG. 3. EoSs of this paper that satisfy observational constraints. We show envelopes for EoSs without FOPT (red) and EoSs with FOPT with different onset density ranges (green and blue), see the details in the text. The shaded bands correspond to stable NS configurations, whereas the solid lines show the EoSs extended beyond the maximally massive NS configurations. The black contour depicts the results of Ref. [38], and the gray contour represents the perturbative QCD constraint.

R. Somasundaram,[1,*] I. Tews,[2] and J. Margueron[1]
PHYSICAL REVIEW C **107**, 025801 (2023)

Maximum mass and maximum density

NS as a laboratory of high density matter

Higher M_{max} - lower density at the center of NS

- $M_{\max} \simeq 1.4\,M_\odot \Rightarrow n_{\rm cent} < 12\,n_0$
- $M_{\max} \simeq 1.7\,M_\odot \Rightarrow n_{\rm cent} < 9\,n_0$
- $M_{\max} \simeq 2\,M_\odot \Rightarrow n_{\rm cent} < 7\,n_0$
- $M_{\max} \simeq 2.25\,M_\odot \Rightarrow n_{\rm cent} < 5\,n_0$
- $M_{\max} \simeq 2.5\,M_\odot \Rightarrow n_{\rm cent} < 4\,n_0$

NS - laboratory of high density:
the range of available densities shrinks

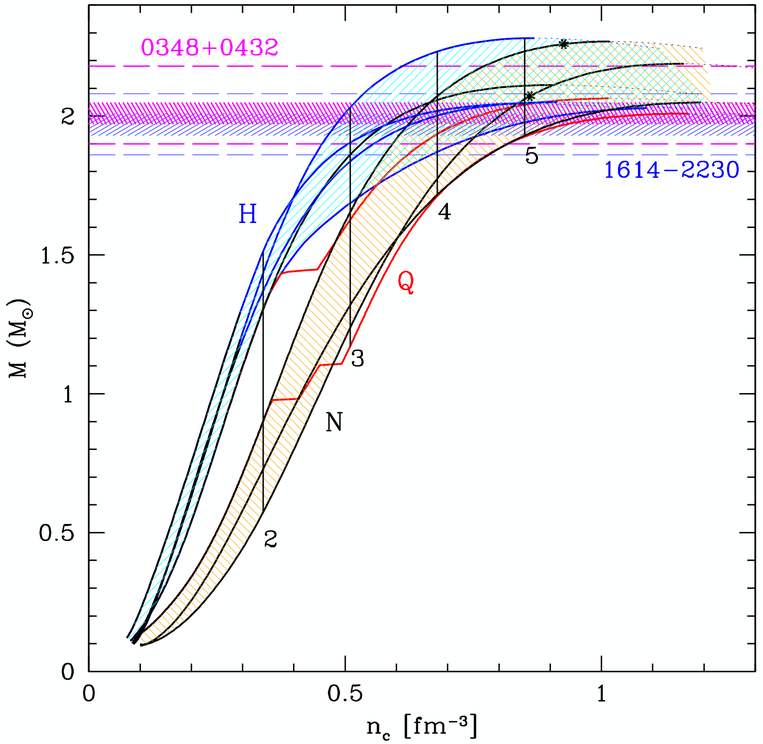

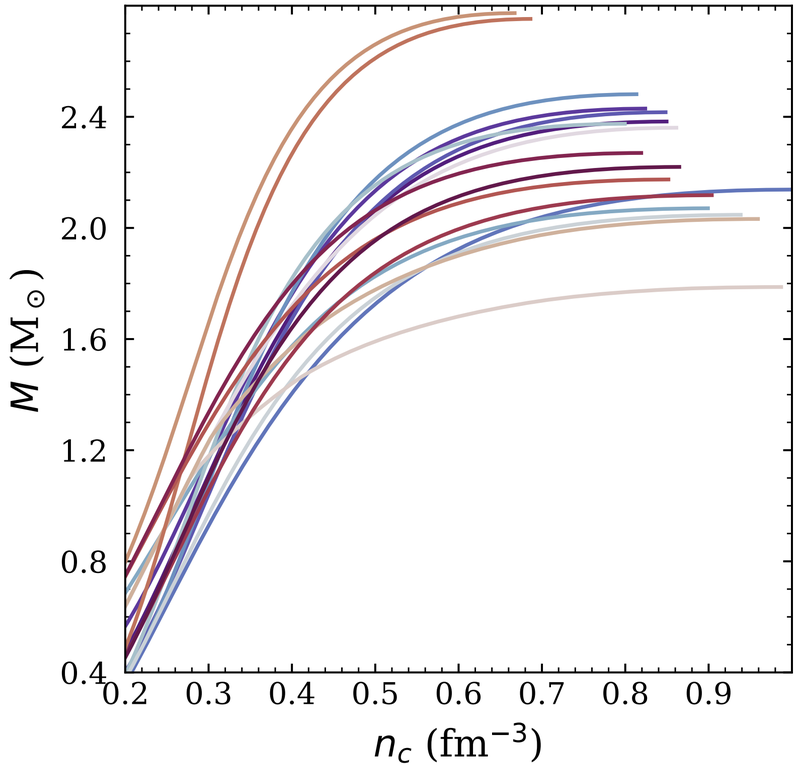

Haensel et. al. Eur. Phys. J. A (2016) 52: 59

Conclusions

- Neutron star mass - the main measurable quantity for constraints on the equation of state
  - relatively high accuracy
  - the role of the maximum mass
- Present limit on the maximum mass (as a condition for rejecting the theory of dense matter) is still

$$M_{\max}(\text{theory}) > 2\,\mathrm{M}_{\odot}$$

- Many models of dense matter consistent with the NS mass measurements (and consistent with nuclear experiments at low density limit)
- Current observations of NS do not impose significant constraints on nuclear parameter
- X-ray observations favor large R in some tension with GW measurement of tidal deformability.
- Confirmation of $\sim 2.3\,\mathrm{M}_{\odot}$ measurement (with higher accuracy) or observation of $M > 2.5\,M_{\odot}$ NS would exclude many soft models od dense matter (including phase transitions to hyperons and quarks in the center).

Perspectives and future missions

- Enhanced X-ray Timing and Polarimetry eXTP - 2027
- Advanced Telescope for High-ENergy Astrophysics ATHENA -2030s
- Square Kilometer Array SKA - radio
- LIGO-Virgo-KAGRA LVK gravitational waves O4, O5 runs
- Einstein Telescope 2030s
- Cosmic Explorer 2030s

and a bit of luck is needed

Massive neutron stars with small radii in relativistic mean-field models optimized to nuclear ground states

Tsuyoshi Miyatsu [1], Myung-Ki Cheoun [1], Kyungsik Kim [2], and Koichi Saito [3]

[1] *Department of Physics and OMEG Institute, Soongsil University, Seoul 06978, Republic of Korea*
[2] *School of Liberal Arts and Sciences, Korea Aerospace University, Goyang 10540, Republic of Korea*
[3] *Department of Physics, Faculty of Science and Technology, Tokyo University of Science, Noda 278-8510, Japan*

ABSTRACT

We present an equation of state (EoS) for neutron stars using the relativistic mean-field model with isoscalar- and isovector-meson mixing. Taking into account the results of the neutron skin thickness, $R_{\rm skin}$, of ^{208}Pb reported by the PREX collaboration, the dimensionless tidal deformability of a canonical neutron star observed from GW170817, and a 2.6 $M_{\odot}$ compact star implied by the secondary component of GW190814, a new effective interaction is constructed so as to reproduce the saturation condition of nuclear matter and the ground-state properties of finite, closed-shell nuclei. We find that the neutron star EoS exhibits the rapid stiffening around twice the nuclear saturation density, which is caused by the soft nuclear symmetry energy, $E_{\rm sym}$. It is also noticeable that the thick $R_{\rm skin}$ from the PREX-2 experiment can be achieved with the small slope parameter of $E_{\rm sym}$ stemming from the isoscalar-meson mixing. Thus, we speculate that the secondary component of GW190814 is the heaviest neutron star ever discovered.

Massive neutron stars with small radii in relativistic mean-field models optimized to nuclear ground states

Tsuyoshi Miyatsu [1], Myung-Ki Cheoun [1], Kyungsik Kim [2], and Koichi Saito [3]

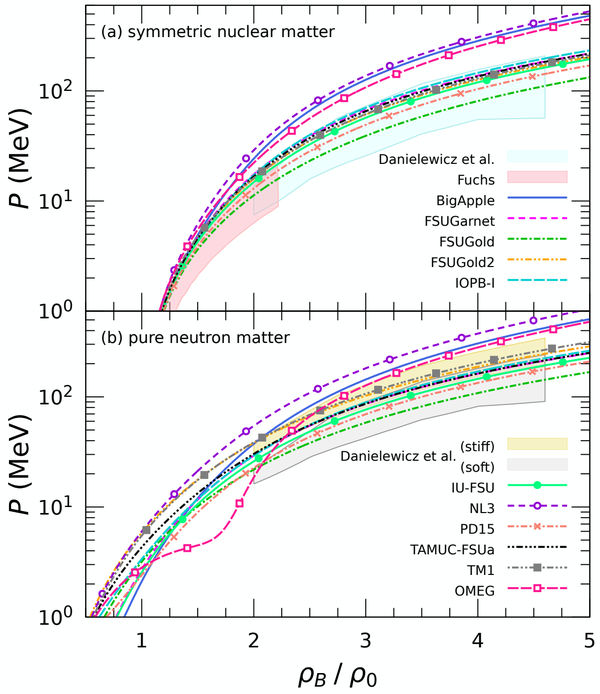

Figure 2. EoS—Pressure, P, as a function of ρ_B/ρ_0—for (a) symmetric nuclear matter and (b) pure neutron matter. The shaded areas represent the constraints from elliptical flow data (Danielewicz et al. 2002) and kaon production data (Fuchs 2006).

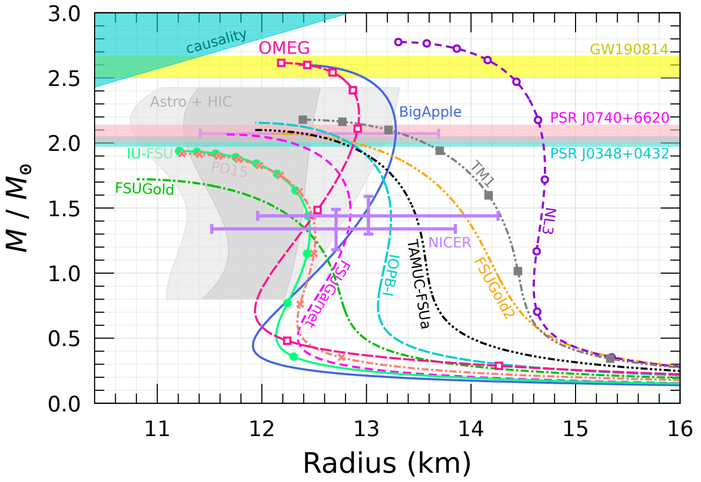

Figure 3. Mass–radius relations of neutron stars. The observational data are supplemented by the constraints from PSR J0030+0451 by a NICER view ($1.44^{+0.15}_{-0.14}$ $M_\odot$ and $13.02^{+1.24}_{-1.06}$ km (Miller et al. 2019) and $1.34^{+0.15}_{-0.16}$ $M_\odot$ and $12.71^{+1.14}_{-1.19}$ km (Riley et al. 2019)), PSR J0348+0432 (2.01 ± 0.04 $M_\odot$) (Antoniadis et al. 2013), PSR J0740+6620 ($2.072^{+0.067}_{-0.066}$ $M_\odot$ and $12.39^{+1.30}_{-0.98}$ km) (Cromartie et al. 2019; Fonseca et al. 2021; Riley et al. 2021), and the secondary object of GW190814 ($2.59^{+0.08}_{-0.09}$ $M_\odot$) (Abbott et al. 2020). The recent theoretical restriction using Bayesian inference is also shown in the shaded region (Huth et al. 2022).

Backbending phenomenon

Signature of the softening of EOS

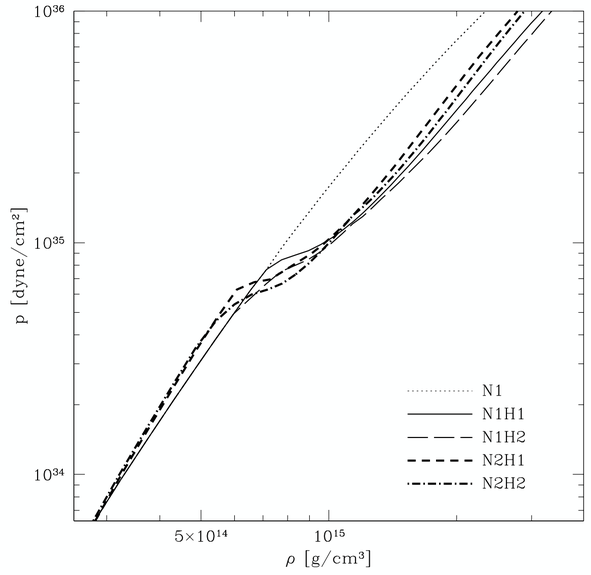

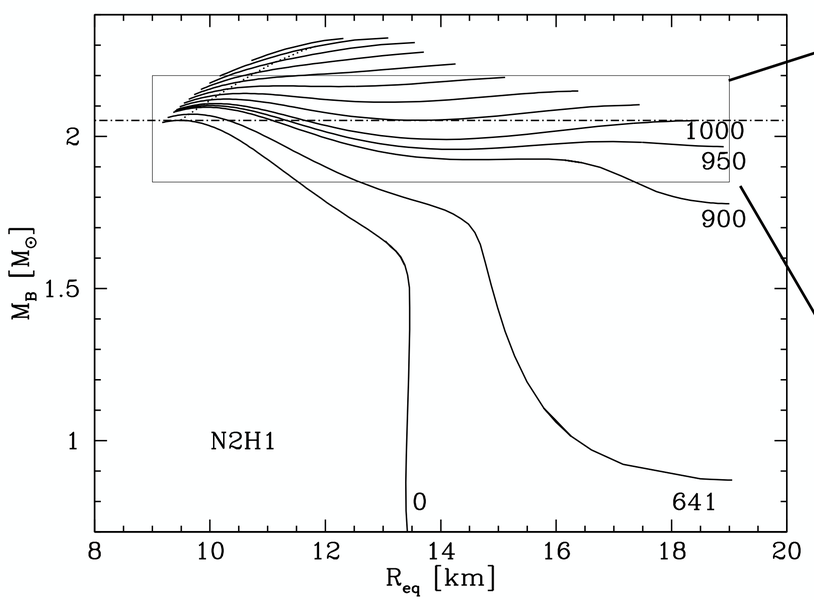

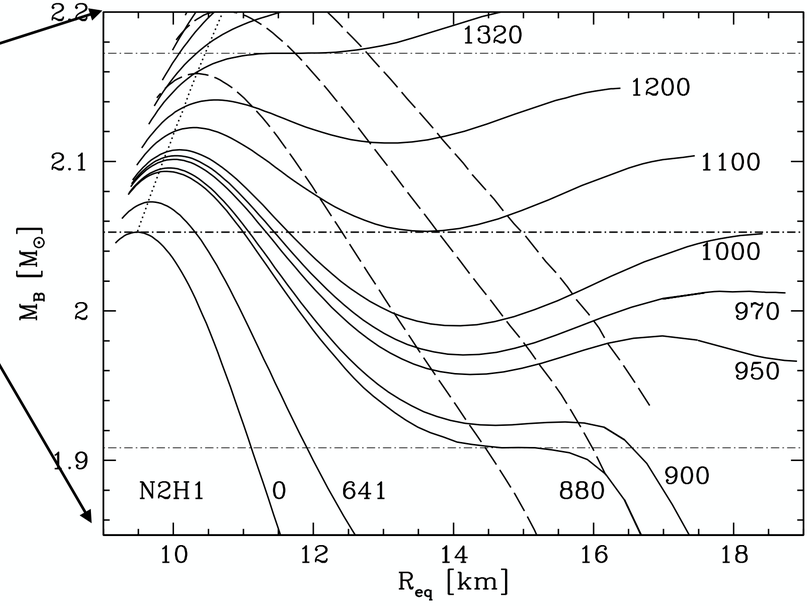

Example of the softening of matter - appearance of hyperons → Change of the slope of $M(R)$ function → Local minima of M at fixed NS rotation

Backbending phenomenon

Spinning-up by angular momentum loss

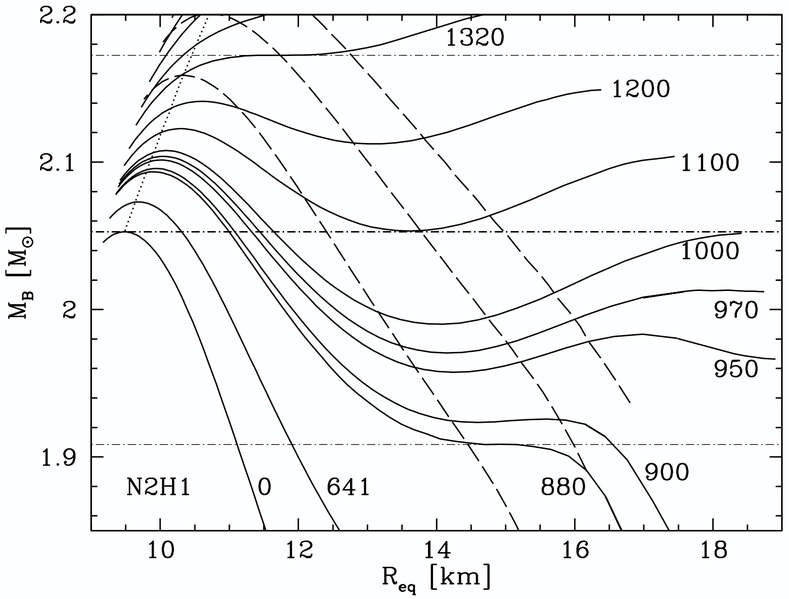

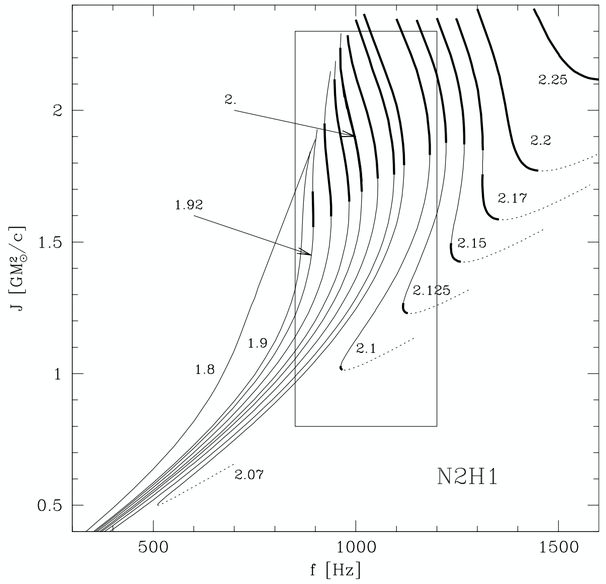

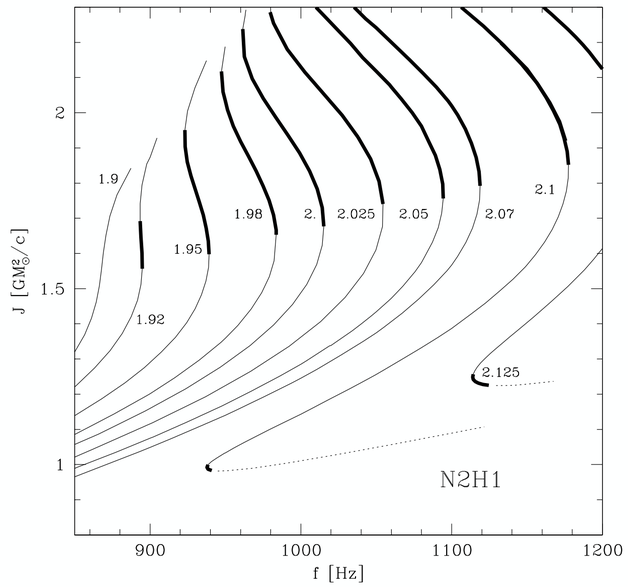

J0952-0607

$$M = 2.35 \pm 0.17\,\mathrm{M}_\odot$$

Table 2
Light-curve/RV-fit Results for J0952[a]

Parameters	Trimmed	All
i (deg)	$59.8^{+2.0}_{-1.9}$	$58.5^{+1.9}_{-1.8}$
f_1	0.79 ± 0.01	0.77 ± 0.01
$L_H\,/10^{34}$ (erg s^{-1})	$3.81^{+0.46}_{-0.43}$	$6.22^{+0.88}_{-0.77}$
T_N(K)	3085^{+85}_{-80}	3206^{+100}_{-95}
d_{kpc}	$6.26^{+0.36}_{-0.40}$	$7.60^{+0.74}_{-0.82}$
χ^2/DoF	286/(298-11)[1.00]	451/(314-11)[1.49]
K_{CoM} (km s^{-1})	376.1 ± 5.1	379.1 ± 6.8
$M_{NS}(M_\odot)$	2.35 ± 0.17	2.50 ± 0.20
$M_C(M_\odot)$	0.032 ± 0.002	0.034 ± 0.002
χ^2/DoF	55/(40-2)[1.4]	90/(43-2)[2.2]

Note.
[a] Also fitted: A_V, Δu, Δg, Δr, Δi, and Δz. See the text.

Inclination: $i = 60^o$

Pulsar mass:

$2.35 \pm 0.17\,\mathrm{M}_\odot \quad \Rightarrow \quad M_{max} > 2.19\,\mathrm{M}_\odot$ at 1σ confidence level

$M_{max} > 2.09\,\mathrm{M}_\odot$ at 3σ confidence level

Companion mass: $0.032 \pm 0.002\,\mathrm{M}_\odot$

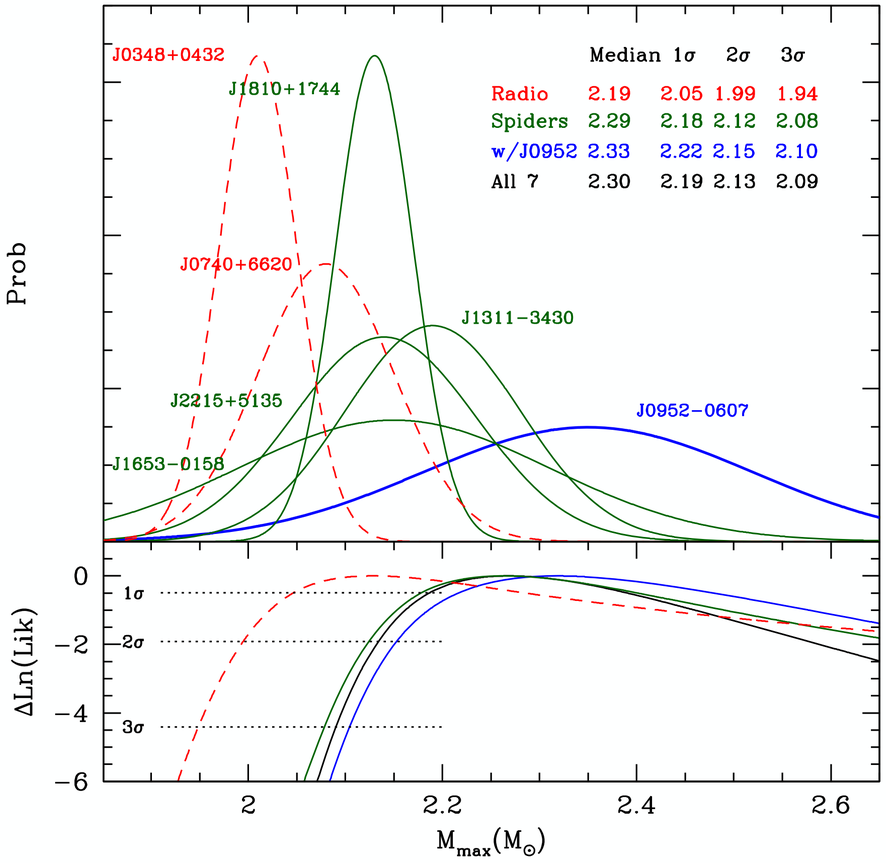

Mass estimates for heavy NSs. The dashed curves show the two heaviest WD–pulsar binaries with masses measured from radio pulse timing (supplemented by WD atmosphere modeling for J0348). The solid curves show the best mass estimates from companion spectroscopy and light-curve fitting for four BWs (J1810, J1653, J1311, and J0952) and one RB (J2215). The bottom panel shows the normalized Ln(Likelihood) for various combinations of these measurements, assuming a flat distribution of masses from 1.8 M_e up to some M_{max}. The inset legend gives the median estimator for M_{max} as well as the 1σ, 2σ, and 3σ lower bounds on its value, for various data subsets.